

## A FLUX-LIMITED SAMPLE OF BRIGHT CLUSTERS OF GALAXIES FROM THE SOUTHERN PART OF THE ROSAT ALL-SKY SURVEY: THE CATALOG AND THE LOGN-LOGS.

S. DE GRANDI<sup>1,2</sup>, H. BÖHRINGER<sup>1</sup>, L. GUZZO<sup>2</sup>, S. MOLENDI<sup>3</sup>, G. CHINCARINI<sup>2,4</sup>, C. COLLINS<sup>5</sup>, R. CRUDDACE<sup>6</sup>, D. NEUMANN<sup>7</sup>, S. SCHINDLER<sup>1,5</sup>, P. SCHUECKER<sup>1</sup>, AND W. VOGES<sup>1</sup>

*Accepted for publication in ApJ: scheduled for the March 20, 1999 issue, Vol. 514.*

### ABSTRACT

We describe the selection of an X-ray flux-limited sample of bright clusters of galaxies in the southern hemisphere, based on the first analysis of the ROSAT All-Sky Survey data (RASS1). The sample is constructed starting from an identification of candidate clusters in RASS1, and their X-ray fluxes are re-measured using the Steepness Ratio Technique. This method is better suited than the RASS1 standard algorithm for measuring flux from extended sources. The final sample is count-rate-limited in the ROSAT hard band (0.5-2.0 keV), so that due to the distribution of  $N_H$ , its effective flux limit varies between  $\sim 3$  and  $4 \times 10^{-12}$  erg cm<sup>-2</sup> s<sup>-1</sup> over the selected area. This covers the  $\delta < 2.5^\circ$  part of the south Galactic cap region ( $b_{II} < -20^\circ$ ) – with the exclusion of patches of low RASS1 exposure time and of the Magellanic Clouds area – for a total of 8235 deg<sup>2</sup>. 130 candidate sources fulfill our selection criteria for *bonafide* clusters of galaxies in this area. 101 of these are Abell/ACO clusters, while 29 do not have a counterpart in these catalogs. 126 (97%) clusters have a redshift and for these we compute an X-ray luminosity. 20% of the cluster redshifts come from new observations, as part of the ESO Key Program REFLEX Cluster Survey that is under completion. Considering the intrinsic biases and incompletenesses introduced by the flux selection and source identification processes, we estimate the overall completeness to be better than 90%. The observed number count distribution, LogN-LogS, is well fitted by a power law with slope  $\alpha = 1.34 \pm 0.15$  and normalization  $A = 11.87 \pm 1.04$  sr<sup>-1</sup> (10<sup>-11</sup> erg cm<sup>-2</sup> s<sup>-1</sup>) <sup>$\alpha$</sup> , in good agreement with other measurements.

*Subject headings:* galaxies: clusters: general — surveys — X-rays: galaxies

### 1. INTRODUCTION

Clusters of galaxies are astrophysical objects carrying fundamental information about the characteristics of the Universe. They are the largest gravitationally bound units, and the time scales involved in their dynamical evolution are comparable to the age of the Universe. Hence clusters are cosmologically young structures, in which evidence of the initial conditions has not yet been totally removed by dissipative effects. On the other hand their dynamical state is approaching a characteristic equilibrium configuration that allows a coherent modeling (e.g. King 1966). Because of these particular properties, the characteristics of the population of galaxy clusters are strongly related to the cosmological parameters. Both theory and simulations have shown that cluster morphologies, comoving densities, and clustering properties provide information on the density parameter,  $\Omega_0$ , and on the shape and normalization of the primordial power spectrum (e.g., Frenk et al. 1990; Bahcall & Cen 1993; White et al. 1993; Kitayama & Suto 1997; Evrard 1997).

To be able to measure such ensemble-averaged quanti-

ties, one needs to select large, statistically complete samples, which have to be representative of clusters of galaxies as a class.

In parallel with deep cluster surveys (e.g. Rosati et al. 1997; Collins et al. 1997; Jones et al. 1998), it is particularly important to accurately define the properties of the cluster population at low redshifts, to provide the reference frame for quantifying cluster evolution. For example, an accurate estimate of the luminosity function, which is an essential part of this statistical analysis, requires the detection of clusters over a fairly large volume of space to reach an accurate evaluation of the bright end of the distribution. On the other hand, a sample of clusters of galaxies covering a large volume of the local Universe, would allow the study of clustering over scales  $\gg 100$  h<sup>-1</sup> Mpc, i.e. around the turnover of the power spectrum. On these scales, these measures would overlap the most recent and future microwave background anisotropy experiments (e.g. Gawiser & Silk 1998), thus providing a direct comparison of the clustering in the light and in the mass.

In recent years it has become ever more evident that the selection of large samples of clusters is best done in the soft

<sup>1</sup>Max-Planck-Institut für extraterrestrische Physik, Giessenbachstraße 1, 85740 Garching bei München, Germany.

<sup>2</sup>Osservatorio Astronomico di Brera, via Bianchi 46, 22055 Merate (LC), Italy.

<sup>3</sup>Istituto di Fisica Cosmica, CNR, via Bassini 15, 20133 Milano, Italy.

<sup>4</sup>Università di Milano, via Celoria 16, 20133 Milano, Italy.

<sup>5</sup>Astrophysics Research Institute, Liverpool John Moores University, Byrom-Street, Liverpool L3 5AF, United Kingdom.

<sup>6</sup>E. O. Hulburt Center for Space Research, Naval Research Laboratory, Code 7620, 4555 Overlook Ave., Washington, DC 29375.

<sup>7</sup>CEA/Saclay, Service d'Astrophysique, L'Orme des Merisiers Bat.709, 91191 Gif-sur-Yvette, France.

X-ray band (i.e. energies in the range from  $\sim 1$  to 10 keV), where clusters are prominent among the various classes of extragalactic objects by virtue of their extremely high X-ray luminosities,  $\sim 10^{43} - 6 \times 10^{45}$  erg s $^{-1}$  (e.g. Böhringer 1995). The X-ray emission originates in the thin hot gas, contained by the deep cluster potential well, in a state approaching the hydrostatic equilibrium (e.g. Sarazin 1988). The predominant emission mechanism at these high energies in clusters is thermal bremsstrahlung, and as the hot gas is distributed throughout the potential well, clusters of galaxies observed in the X-ray band appear, unlike at optical wavelengths, as single diffuse entities. Moreover, as the X-ray intensity scales quadratically with the gas density, whereas the integrated optical luminosity is only linearly correlated with the galaxy density, observations in the X-ray band are less subject to the projection effect problems which affect optically selected catalogs of galaxy clusters.

A unique opportunity to construct large cluster samples selected in the X-ray band has been provided by the ROSAT mission (Trümper 1993). This satellite conducted, in the second half of 1990, an all-sky survey in soft X-rays (0.1-2.4 keV) with the Position Sensitive Proportional Counter (PSPC; Briel & Pfeffermann 1986) as focal plane detector. Due to the improved spatial resolution, the higher sensitivity, and the smaller intrinsic background with respect to previous X-ray satellites, ROSAT data are especially attractive for the study of clusters of galaxies. Furthermore, the ROSAT All-Sky Survey (RASS) is the first conducted with an imaging X-ray telescope and is uniquely suited to obtaining complete X-ray cluster samples over large areas of the sky. Several approaches to the problem of selecting statistical samples of galaxy clusters from the RASS1 database have been described (e.g. Burg et al. 1992; Briel & Henry 1993; Romer et al. 1994; Ebeling et al. 1996, 1997).

In 1992 an ESO Key Program (hereafter ESOKP; Böhringer 1994; Guzzo et al. 1995) was started with the aim of constructing in the southern sky the largest flux limited sample of clusters of galaxies using the RASS. Due to the huge number of X-ray sources detected, more than 50000 objects, it was not feasible to start an observing campaign with the aim of optically identifying all the RASS sources in the southern hemisphere. However, it is generally assumed that mass fluctuations on scales of a few to tens of Megaparsecs lead to the formation of clusters of galaxies visible optically and in the X-ray band. Therefore the approach followed by the ESOKP collaboration is to search for correlations between X-ray sources with regions of galaxy overdensity. The resulting list is then correlated with catalogs such as the NASA Extragalactic Data Base (NED) and SIMBAD, in order to remove chance correlations with stars and AGNs. The final step is to observe the refined list spectroscopically, in order to derive the cluster redshift, if not already known, and to remove some remaining sources which are not clusters.

As discussed in De Grandi et al. (1997, Paper I hereafter), however, the standard analysis (see § 2.1) performed on the RASS data is not fully appropriate for characterizing extended sources. In particular, fluxes are systematically underestimated. These limitations have prompted the development of alternative techniques such as the Steepness Ratio Technique (SRT), discussed in Pa-

per I, and the Voronoi Tessellation and Percolation analysis (Ebeling et al. 1996). Here, we present the application of the SRT to an initial set of candidate clusters from the ESOKP, that leads to the construction of a complete flux limited sample of bright clusters of galaxies. The sample is limited to the southern Galactic cap region ( $b_{II} < -20^\circ$ ,  $\delta < 2.5^\circ$ ), and its X-ray and optical completeness are investigated in detail. In addition, we shall also compute and discuss the LogN-LogS distribution.

A preliminary version of the sample presented here, was previously used to obtain an estimate of the cluster X-ray luminosity function (XLF, De Grandi 1996b). An updated estimate of the XLF from the present catalog is the subject of a parallel paper (De Grandi et al. 1999). These results will be extended by the future developments of the ongoing ESOKP collaboration (now known as the REFLEX Cluster Survey, see Böhringer et al. 1998).

The paper is organized as follows. In § 2 we describe briefly the RASS1 data used to derive the X-ray source properties and the various algorithms applied to these data. In § 3 we describe the initial procedures used by the ESOKP collaboration to define a sample of clusters in the southern hemisphere using the RASS1 data, which we call here the RASS1 Candidate Sample. The procedure for the selection and definition of the sample of bright clusters, which we shall call the RASS1 Bright Sample, is presented and discussed in detail in § 4. In § 5 we compute the number counts, or LogN-LogS distribution, of this sample, and compare it with previous results. In § 6 we investigate the potential biases that could affect the RASS1 Bright Sample. In § 7 we summarize our main results and conclusions.

## 2. ANALYSIS OF ROSAT ALL-SKY SURVEY SOURCES

### 2.1. SASS1 analysis of strip data

The first analysis of the ROSAT All-Sky Survey sorted the data into 90 great-circle strips on the sky, each  $2^\circ$  wide and passing through the ecliptic poles. These strips were processed one by one by using the Standard Analysis Software System (SASS1; e.g., Voges 1992) developed at MPE (Germany). The detection process used photons in the broad PSPC energy band 0.1-2.4 keV. Each data strip was analyzed using a combination of source detection algorithms, including two *sliding window* techniques (the first using a local background determination, the latter a global background map) and a Maximum Likelihood (ML) method (Cruddace et al. 1988). SASS1 produced an all-sky source catalog of  $\sim 50.000$  objects (with existence likelihood larger than 10) containing information about source properties, such as detection significance, count rate, position, hardness ratio and extent. As explained in § 3 the first candidate sample for the ESOKP, on which the present work is based, was selected from this catalog.

### 2.2. Analysis of merged data

As mentioned in the introduction, our first goal was to re-estimate using the SRT approach the X-ray fluxes for all candidate clusters, selected from the SASS1 source list. After the end of the survey, it was possible to obtain from the ROSAT team  $2^\circ \times 2^\circ$  sky fields, centered on the SASS1 ML positions, containing the photons accumulated from all the overlapping strips, known as *merged data*. We col-

lected the merged data fields for all our cluster candidates and first analyzed them using the standard detection procedure, as implemented in the EXSAS package (Zimmermann et al. 1997). The first aim of this was to re-estimate the source positions with the ML algorithm with improved accuracy. The standard analysis on the merged data was performed in the three ROSAT PSPC energy bands: the broad band (0.1-2.4 keV), the soft band (0.1-0.4 keV) and the hard band (0.5-2.0 keV). A detailed description of this analysis can be found in Paper I.

We proceeded then by applying the SRT to the merged data using the new ML position. We recall here that SRT uses the convolution between the real RASS point-spread function (G. Hasinger 1995, private communication) and a  $\beta$ -model of the cluster emission profile (with parameter  $\beta$  fixed to 2/3),  $\tilde{I}(r)$ , to derive for each cluster the core radius and the total count rate. We compute for each source the observed steepness ratio,  $SR_{obs}$ , that is the ratio between the source counts within an annulus bounded by the two radii of 3 and 5 arcmin and those within a 3 arcmin radius circle. The source core radius is derived by comparing  $SR_{obs}$  with the theoretical  $SR = \int_{3'}^{5'} 2\pi r \tilde{I}(r) dr / \int_{0'}^{3'} 2\pi r \tilde{I}(r) dr$ , as a function of the core radius (Figure 5 in Paper I). The total source counts are computed by correcting the measured counts within 5 arcmin radius, by the fraction falling outside this aperture, by means of an  $SR_{obs}$  dependent correction factor  $F$ , shown in Figure 8 of Paper I. SRT also evaluates the probability for each source to be pointlike, which is computed without using a specific model for the source emission profile. The SRT analysis was performed in all three ROSAT PSPC energy bands.

### 3. THE RASS1 CANDIDATE SAMPLE

As soon as the ROSAT All-Sky Survey went through its first processing (SASS1), an automatic identification program for galaxy clusters in the Southern sky was set-up as a collaboration between MPE and ROE/NRL. The broad aim of this work was to identify all SASS1 X-ray sources that could possibly be associated with a cluster of galaxies, known or unknown from available optical cluster catalogs. Given the detection limit of the RASS, the redshift distribution of the identified clusters was expected to peak between 0.1 and 0.2 in redshift, so that the bulk of the rich cluster population was clearly detectable on the ESO/SRC survey plates.

The main identification method was therefore to look for overdensities of galaxies in the ROE/NRL object catalog, produced by digitizing the IIIa-J plates with the COSMOS machine in Edinburgh (Yentis et al. 1992), around each SASS1 source above a given SASS1 count rate (see below). An excess probability could thus be defined by comparison with counts at random positions and well characterized thresholds in completeness and contamination could be defined. Relatively low search thresholds in contamination were used to avoid discarding genuine X-ray clusters, leading to the inclusion in the candidate list also of spurious objects that had to be removed in a later step of the work. As a further complement to this, the SASS1 source list was also correlated with the Abell/ACO catalog of clusters of galaxies (Abell et al. 1989) and with

a catalog of automatic clusters independently constructed from the COSMOS galaxy database.

The third method was to include also all the sources flagged by SASS1 as having an extent radius  $> 25$  arcsec and an extent likelihood  $> 7$ . This is the only method which is based on the X-ray properties alone. Its main drawback is that of not being particularly robust, so that some truly extended sources are not recognized as such. In addition, the RASS data are not optimal in general for recognizing extended sources, due to the low photon statistics that couples with the limited resolution of the RASS. Despite its limitations, however, this technique complements the optically-based methods, and (§6.2), provides a useful way to roughly estimate the completeness of the identification process. Finally, the three cluster candidate lists were merged and multiple X-ray detections of the same object were removed, for a total of  $\sim 1000$  objects. In this paper we consider only southern sky candidates at high Galactic latitudes,  $\delta < 2.5^\circ$  and  $b_{II} < -20^\circ$ , leading to a sample of 679. This list will be referred to as the RASS1 Candidate Sample.

As mentioned above, prior to the identification procedure, the initial sample of sources from RASS1 was thresholded to a count rate limit of 0.055 cts/s. Due to a problem in the early processing of the data, however, the count rate in a few strips had a systematic shift, so that in the end they were thresholded to a higher limit, 0.08 cts/s. This problem, discovered later in the course of our analysis, affected 17% of the total sample. We shall show in the following how this residual incompleteness has been taken into account.

### 4. SELECTION OF THE RASS1 BRIGHT SAMPLE

In this section we describe how we proceeded in order to select a flux limited sample of clusters of galaxies from the RASS1 Candidate Sample. To this end we must first consider the possible sources of incompleteness that could affect the sample.

#### 4.1. Exposure Times and Sky Area Selections

A first source of incompleteness derives from the differences in exposure times over the different strips, which in the southern sky may vary between 0 and  $\sim 800$  seconds, with a peak at  $\sim 400$  seconds. In Figure 1 we plot the SASS1 broad band count rates versus the SASS1 exposure times for the RASS1 Candidate Sample. We separate the pointlike sources (asterisks) from the extended ones (open circles) by using the SRT probability of extension: we define as extended any source with a probability of being pointlike  $< 1\%$ . The solid and dotted lines drawn in Figure 1, correspond to the count rate limits of 0.055 cts/s and 0.08 cts/s discussed at the end of § 3, respectively. Note how for both count rate limits, SASS1 starts to fail in detecting sources when the exposure time becomes smaller than  $\sim 100 - 120$  s. Therefore, we consider only regions with exposures larger than 150 seconds, in order to avoid regions of the sky where objects could have been missed because of the low sensitivity of the survey.

To avoid incompleteness problems related to the difficulty in identifying clusters inside optically crowded fields, we also excluded the sky areas of the Galactic plane and the Magellanic Clouds. The Galactic plane region was in

fact already excluded in the early selection of the RASS1 Candidate Sample to avoid regions of high  $N_H$  values, by selecting only sources with  $b_{II} < -20^\circ$ . To establish the size of the area to be excluded in the case of the Magellanic Clouds, we considered both the optical and the X-ray Cloud emission (e.g. Snowden & Petre 1994). We opted for a conservative choice rejecting an area slightly larger than that covered by both the emissions. The lower left and upper right corners of the excluded areas in equatorial coordinates (J2000.0) are  $\alpha_{ll} = 93.135^\circ, \delta_{ll} = -77.5167^\circ$  and  $\alpha_{ur} = 60.1783^\circ, \delta_{ur} = -62.3611^\circ$  for the LMC, and  $\alpha_{ll} = 22.663^\circ, \delta_{ll} = -77.243^\circ$  and  $\alpha_{ur} = 353.223^\circ, \delta_{ur} = -67.224^\circ$  for the SMC, respectively.

After excluding these areas and setting a threshold for the exposure time we are left with the geometric area of  $8235 \text{ deg}^2$  (i.e., 2.5 sr), which is shown in Figure 2. This is about a fifth of the whole sky, or a third of the sky available at  $|b_{II}| > 20^\circ$ . The number of cluster candidates in this area is 540.

#### 4.2. Count Rate Selection

In § 3 we discussed how the RASS1 Candidate Sample was selected, starting from the list of X-ray sources detected in the survey by SASS1. However this initial selection procedure was lacking in two respects. First, a flux threshold should be set using count rates in the ROSAT hard band (0.5-2.0 keV), which is best suited for the analysis of hard sources such as clusters, whereas initially thresholds were set using SASS1 count rates in the broad band (0.1-2.4 keV). Second, the SASS1 algorithm, designed for speed, was rather imprecise in estimating the flux and angular extent of clusters (Paper I; Ebeling et al. 1996), a problem the SRT algorithm was designed to correct. In this section we select bright clusters from the RASS1 Candidates Sample by means of a cut in SRT count rate computed in the hard band. We show that a limiting SRT count rate of 0.25 cts/s leads to a sample characterized by a high degree of completeness.

##### 4.2.1. Study of a Control Sample

In order to understand the effects of changing the energy band and introducing a further count rate selection using SRT results we investigate the behavior of a control sample of sources, obtained from the *Einstein* Extended Medium Sensitivity Survey (EMSS; Gioia et al. 1990; Maccacaro et al. 1994) and reobserved in the RASS. No cut in SASS1 count rates has been applied to this dataset. Out of the 835 EMSS objects we selected two samples, the first comprising pointlike sources, i.e. objects classified as AGNs, BL Lac and stars (Maccacaro et al. 1994), and the second potentially extended sources, i.e. objects classified as galaxies or clusters of galaxies. For both samples we include only objects detected in the RASS1 merged data by the ML algorithm (see § 2.2) in the broad band, with an ML existence likelihood larger than 12. These selections lead to well defined EMSS control samples of 108 pointlike and 50 potentially extended objects.

In Figure 3 we show the comparison between the SRT hard band count rates and the SASS1 broad band count rates for the EMSS pointlike (asterisk) and potentially extended (open circles) sources. The observed distribution

allows us to estimate how many sources would be lost in passing from one X-ray analysis system to the other. The sources lost due to the SASS1 count rate cut applied prior to the SRT analysis should fall in the top left quadrant delimited by the dotted vertical and horizontal lines representing the cuts of 0.055 cts/s and 0.25 cts/s, respectively. Since no pointlike sources are present in the top left quadrant, we deduce that the degree of completeness of a sample of pointlike sources with a threshold in the SRT hard band count rate of 0.25 cts/s, previously cut with a SASS1 broad band count rate of 0.055 cts/s, is extremely high. Two “extended” objects fall in the top left quadrant, indicating that the completeness of the corresponding sample of extended sources, although still quite high, is not 100%. The difference between the distribution of pointlike and extended sources in the count rate plane is produced by the strong underestimation of the count rate by SASS1 for extended sources (see § 4.2).

##### 4.2.2. Study of the RASS1 Candidate Sample

In the light of the results described above we examine now our list of cluster candidates. As we mentioned in § 3, this is divided into two distinct subsamples characterized by two SASS1 broad band count rate limits (0.055 and 0.08 cts/s). We call the first SUB1 and the second SUB2. SUB1 is not only deeper but also more populated (83% of the total RASS1 Candidate Sample). In Figure 4 we plot for SUB1 the SRT hard band against the SASS1 broad band count rates. The horizontal and vertical dashed lines correspond to the count rate limits of 0.25 and 0.055 cts/s, respectively. The sources we miss when cutting the SUB1 sample at an SRT hard band count rate of 0.25 cts/s, because of the prior SASS1 cut, are those which would populate the top left quadrant. We have used the observed distribution of points in Figure 4 to estimate the number of missed sources. After selecting the SUB1 sources with  $cr_{SRT} > 0.25 \text{ cts/s}$  (133 sources), we have plotted the distribution of their SASS1 count rates. This is shown in logarithmic bins in Figure 5. The histogram has a maximum for  $cr_{SASS1} \sim 0.25 \text{ cts/s}$ , and clearly, the decrease below this value is produced by the applied SRT cut. The number of missed sources in the top left quadrant of Figure 4 can then be estimated extrapolating the distribution below the  $cr_{SASS1}$  cutoff. A linear extrapolation, using the four bins nearest to the SASS1 limit, gives a number of missing sources equal to  $\sim 1.5_{-1.5}^{+5.4}$ . In order to be conservative we will take the upper bound of this result, and assume that 6.9 sources are lost.

We now wish to estimate the sources we miss when cutting the SUB2 sample at SRT count rate of 0.25 cts/s, because of the prior SASS1 cut. The number of SUB2 sources above  $cr_{SRT} = 0.25 \text{ cts/s}$  is 31. The number of SUB2 sources which should be falling within the SASS1 count rate range 0.055 – 0.08 cts/s can be directly estimated from the observed distribution of SUB1 sources: 8 objects of SUB1 fall within the SASS1 range 0.055–0.08 cts/s, corresponding to  $\sim 1.9$  objects in SUB2. The number of SUB2 sources which should be falling below  $cr_{SASS1} = 0.055 \text{ cts/s}$  (i.e.,  $\sim 1.3$  objects) can then be derived using that estimated for SUB1. Adding all these contributions, we estimate that for the whole RASS1 Candidate Sample, the expected missing sources amount to  $\sim 8.6$  (i.e.  $\sim 5\%$  of

the total sample). We therefore expect the sample to be  $\sim 95\%$  complete as far as the X-ray selection is concerned. Such a high degree of completeness has been achieved at the price of reducing drastically the number of sources: the RASS1 Candidate Sample contained 679 objects, while this sample contains now 164 candidates.

#### 4.3. Definition of the RASS1 Bright Sample

As a result of the selections described in the previous subsections we obtain a list of 164 cluster candidates. In order to assign a reliable classification to these objects we have collected the following information: 1. images from the Southern Digitized Sky Survey (SDSS); 2. overlays of X-ray contours on optical object distributions from the COSMOS catalog; 3. information from the NED and SIMBAD databases; 4. X-ray properties, such as source extent, probability of extent, X-ray flux and luminosity from RASS1 data and ROSAT pointed data when available; 5. optical CCD images and spectra from the ESOKP. Redshifts were obtained from the literature and from our new ESOKP observations.

The analysis of this information allowed us to divide the cluster candidates into 4 groups:

- (A) confirmed clusters of galaxies, i.e. objects for which the inspection of optical images and spectra allow a certain identification of the X-ray source with a cluster;
- (B) likely clusters, i.e. objects with X-ray and optical properties consistent with clusters, lacking firm spectroscopic confirmation;
- (C) uncertain identifications, i.e. objects for which either we have insufficient information to discriminate between two possible classifications or we have no information at all;
- (D) objects which are certainly not galaxy clusters (27 obj.).

This classification into the four classes was done independently three times to reduce subjective definitions, and the agreement was excellent.

The rather high degree of contamination was expected as a result of the pre-selection methods we have applied in constructing the RASS1 Candidate Sample.

In paper I we pointed out that for very extended sources the source profile appears to be almost flat between 0 and 5 arcmin and the observed steepness ratio approaches its maximum value (i.e. the ratio between the areas of the annulus bounded by 3 and 5 arcmin and of the circle of 3 arcmin radius). This large observed steepness ratio leads to diverging values of the core radius, the total source counts and the associated uncertainties. To overcome this effect we impose that the physical core radius (in kpc) of a cluster candidate cannot be larger than a certain upper limit. If the physical core radius found by SRT is larger than the limit we compute a new angular core radius from the limiting core radius using the redshift of the source, derive the corresponding steepness ratio (see Figure 5 in Paper I), and finally, with the new steepness ratio and the curve shown in Figure 7 in Paper I, we compute the revised count

rate of the source. The average core radius of rich clusters is about 250 kpc (Bahcall 1975), while Jones and Forman (1984) found that out of 38 clusters 80% have a core radius smaller than 300 kpc and only 20% have a core radius in the range 300 and 800 kpc. Various tests with different values of the physical core radius show that the best compromise is achieved with a value of 400 kpc for the upper limit of the core radius. 21 sources belonging to classes A, B and C have a modified SRT count rate, but for 14 only the revised count rate differs by more than 10% from its original value. Moreover, 7 sources have a revised SRT count rate that falls below our threshold of 0.25 cts/s and therefore leave the sample.

We define as the RASS1 Bright Sample the sum of sources belonging to the A (119), B (6) and C (5) groups, using the results of the revised SRT. The final sample contains 130 sources. A schematic representation of the selections leading to the construction of the RASS1 Bright Sample from the RASS1 Candidate Sample is given in Figure 6.

#### 4.4. The Catalog of X-ray sources

The sources of the RASS1 Bright Sample are presented in Table 1. Columns list the observed and derived parameters for each source as follows:

*Column (1).* — Sequence number of the source in the catalog.

*Column (2).* — Position: right ascension (hh mm ss.s, first line) and declination (dd mm ss.s, second line) as derived by the ML algorithm when analyzing the RASS1 merged data (J2000.0 coordinates).

*Column (3).* — Column density of Galactic Hydrogen from Dickey & Lockman (1990) in units of  $10^{20}$  atoms  $\text{cm}^{-2}$ .

*Column (4).* — Vignetting corrected RASS1 exposure time computed from merged data in seconds.

*Column (5).* — Source count rate (first line) computed in a circle of 5 arcmin radius from the source position in the PHA channels from 52 to 201 (corresponding to the 0.5-2.0 keV energy band), and  $1-\sigma$  errors (second line) from photon-counting statistics.

*Column (6).* — Total SRT source count rate (first line) in the 0.5-2.0 keV band and associated uncertainties (second line).

*Column (7).* — Model independent probability of the source to be pointlike. Sources with probability smaller than 1% are considered extended.

*Column (8).* — Unabsorbed X-ray flux (first line) computed in the 0.5-2.0 keV band in units of  $10^{-11}$  erg  $\text{cm}^{-2}$   $\text{s}^{-1}$ , and associated symmetrized  $1-\sigma$  uncertainties (second line).

*Column (9).* — X-ray luminosity (first line) computed in the 0.5-2.0 keV band in units of  $10^{44}$  erg  $\text{s}^{-1}$ , and associated  $1-\sigma$  uncertainties (second line). The luminosity has been computed in the rest frame of the source by assuming a power law spectrum with energy index 0.4,  $H_0 = 50$  km  $\text{s}^{-1}$   $\text{Mpc}^{-1}$  and  $q_0 = 0.5$ .

*Column (10).* — Optical identification. Name of the source (first line), if already known, and proposed classification (second line) according to the description given in §4.3.

*Column (11).* — Source redshift (first line) and associated reference (second line).

*Column (12).* — Comments: contains miscellaneous information on the source.

In Table 2 we list the sources belonging to class D (i.e. non-cluster objects discarded from the RASS1 Bright Sample). The contents of Table 2 are:

*Column (1).* — Optical name of the source if already known.

*Column (2).* — Right ascension (J2000.0 coordinates) of the X-ray source from RASS1 merged data.

*Column (3).* — Declination (J2000.0 coordinates) of the X-ray source from RASS1 merged data.

*Column (4).* — Unabsorbed X-ray flux computed in the 0.5-2.0 keV band with SRT, in units of  $10^{-11}$  ergs  $\text{cm}^{-2}$   $\text{s}^{-1}$ .

*Column (5).* — Uncertainties associated to the X-ray flux in the same units and energy band as in column (4).

*Column (6).* — Source type. STA = star, GAL = “normal” galaxy, GC = globular cluster, AGN = Active Galactic Nucleus (Quasar, Seyfert galaxy or BL Lac object).

#### 4.5. Extent of Clusters in the Catalog

For each cluster of the RASS1 Bright Sample we have computed the probability to be a pointlike source following the SRT method described in Paper I. We find that about 60% of the clusters belonging to the RASS1 Bright Sample can be confidently defined as extended sources, while the remaining  $\sim 40\%$  are consistent with being pointlike. If the RASS1 Candidate Sample had been selected on the basis of source X-ray extent this would have introduced a severe incompleteness in any flux limited sample. Indeed even at a hard band count rate limit of 0.25 cts/s (roughly corresponding to a flux limit of  $\sim 3.5 \times 10^{-12}$  erg  $\text{cm}^{-2}$   $\text{s}^{-1}$ ), almost half of the sources would have been lost. This is due to the limited angular resolution of the RASS, in which a significant fraction of the more distant clusters do not appear as extended sources, coupled to the low photon statistics characterizing RASS sources.

### 5. THE NUMBER COUNTS OF THE RASS1 BRIGHT SAMPLE

#### 5.1. Converting Count Rate to Flux

To convert a count rate into an X-ray flux in the 0.5-2.0 keV band, we assume that all clusters have a thermal spectrum (Raymond & Smith model in XSPEC version 9.01) with a temperature of 5 keV, a metal abundance of  $0.5 Z_{\odot}$  and a redshift of 0.1, which is the median redshift of the RASS1 Bright Sample. The assumption of a spectral model and its associated parameters ( $T$ ,  $Z$  and  $z$ ) is not critical, as the flux in the 0.5-2.0 keV band depends only weakly on these parameters. We find that by varying them within a range of values that are typical for clusters of galaxies ( $T_{\text{gas}} \sim 3 - 10$  keV,  $Z \sim 0.3 - 1.0 Z_{\odot}$ ) and for a reasonable redshift range ( $z \leq 0.3$ ), the conversion factor for the ROSAT hard band changes by less than 5%.

With these assumptions we find that the relation between count rate and flux as a function of  $N_H$  is well fitted, for  $N_H$  in the range  $7 \times 10^{19} - 4 \times 10^{21}$   $\text{cm}^{-2}$ , by a quadratic relation (see also De Grandi 1996a):

$$S = (1.193 + 3.315N_H + 2.152N_H^2) \cdot cr, \quad (1)$$

where  $S$  is the 0.5-2.0 keV flux in units of  $10^{-11}$  erg  $\text{cm}^{-2}$   $\text{s}^{-1}$ ,  $N_H$  is the Galactic absorption for the individual cluster as given in Dickey & Lockman (1990) in units of  $10^{22}$   $\text{cm}^{-2}$  and  $cr$  is the SRT hard band count rate.

#### 5.2. Sky Coverage and LogN-LogS Distribution

Our sample has been obtained by performing a cut in count rate. Since different regions of the sky show different amounts of Galactic absorption, the cut in count rate translates into a range of flux limits. We have computed the flux limit as a function of  $N_H$  and from that we have derived the sky coverage as a function of the flux limit (see Figure 7). As regions of high Galactic absorption have been excluded from the RASS1 Bright Sample (§ 4.1),  $N_H$  varies within a limited range,  $10^{20} < N_H < 10^{21}$   $\text{cm}^{-2}$ . Consequently, the flux limit does not vary much over the available sky area, so that the sky coverage (see Figure 7) is almost constant for flux limits larger than  $\sim 4 \times 10^{-12}$  erg  $\text{cm}^{-2}$   $\text{s}^{-1}$  and decreases rapidly to zero at the flux limit of  $3.05 \times 10^{-12}$  erg  $\text{cm}^{-2}$   $\text{s}^{-1}$ .

The flux limit should take into account exposure time and in the case of clusters the angular extent, e.g., Rosati et al. (1995). However, in our case both of these dependencies may be neglected. As long as the exposure time is larger than 150 seconds (§ 4.1) and the extension is less than  $\sim 4$  arcmin (§ 6.1) a source with an SRT hard band count rate  $> 0.25$  cts/s will be detected.

The cumulative LogN-LogS distribution for the 130 objects of the RASS1 Bright Sample has been computed by summing up the contribution of each cluster weighted by the area in which the cluster could have been detected:

$$N(> S) = \sum_{S_i > S} \frac{1}{\Omega_i}, \quad (2)$$

where  $N(> S)$  is the surface number density of sources with flux larger than  $S$ ,  $S_i$  is the flux of the  $i^{\text{th}}$  source and  $\Omega_i$  the associated solid angle. The LogN-LogS distribution is plotted in Figure 8.

We have modeled the LogN-LogS distribution with a power law of the form:

$$N(> S) = AS^{-\alpha}, \quad (3)$$

and computed the power law slope,  $\alpha$ , using the maximum likelihood method described in Crawford et al. (1970) and Murdoch et al. (1973), which uses the unbinned data. The likelihood function,  $\mathcal{L}$ , is given in the appendix of Murdoch et al. (1973). The derived value for  $\alpha$  ( $1.37 \pm 0.15$ ) has been corrected by the factor  $(M-1)/M$  (Crawford et al. 1970), where  $M$  is the number of objects in the sample, and for the bias in the derived slope induced by the presence of measurement errors in the fluxes (Murdoch et al. 1973, Table 5). This last correction is computed by Murdoch et al. (1973) for the case of noise-limited flux measurements, however, because of the way our sample has been selected, the minimum S/N is not well defined. On the basis of an analysis of the overall S/N distribution, we have defined an effective limiting S/N ( $\sim 8$ ) corresponding to the peak of the distribution and we have applied the correction appropriate for this value. The corrected value of the slope

is  $\alpha = 1.34 \pm 0.15$ , where the quoted errors are  $1\text{-}\sigma$ . The cumulative effect of the two corrections shifts the value of the slope by an amount which is much smaller than the errors. We note that the observed slope is consistent within  $1\text{-}\sigma$  with the Euclidean slope. The normalization,  $A$ , has been computed by imposing that the integral distribution,  $N(> S)$ , described by the power law, be equal to the observed one at the flux of the weakest cluster in the sample. The derived value is  $A = 11.87 \pm 1.04 \text{ sr}^{-1} (10^{-11} \text{ erg cm}^{-2} \text{ s}^{-1})^\alpha$ . Since the maximum likelihood method does not establish whether a model is acceptable, we have applied a Kolmogorov-Smirnov (KS) test to our data. In the case of a power law with slope  $\alpha$  equal to the one derived above the KS test yields a probability of 0.77 for the observed distribution to be extracted from the parent population, indicating that a power law describes adequately our data.

If the best-fit power law is drawn over Figure 8 it appears to be above the data for all the fluxes higher than about  $0.6 - 0.7 \times 10^{-11} \text{ erg cm}^{-2} \text{ s}^{-1}$ . This effect is due to the different statistical weight given to the data points by the maximum likelihood algorithm used for the fitting procedure and to the fact that the distribution reported in Figure 8 is cumulative. Indeed by plotting the differential LogN-LogS this effect disappears indicating its purely statistical nature.

We have performed an internal consistency test by computing the LogN-LogS distribution and the best-fit power law for the 119 sources classified as certain clusters (A) only. The best fit parameters,  $\alpha = 1.32 \pm 0.15$  and  $A = 11.14 \pm 1.01$ , are in agreement with those found by considering the whole sample. Moreover, a KS test between the flux distribution of the sources classified as A and the sources in the B and C groups, did not show any evidence of a statistically significant difference between the two sub-samples.

Figure 8 also shows a comparison of our LogN-LogS distribution with other works. The points shown in Figure 8 are our data, while the long-dashed box and the cross represent the EMSS LogN-LogS (Henry et al. 1992) as recalculated by Rosati et al. (1995) and the Piccinotti et al. (1982) point, respectively. The solid line corresponds to the number counts of the Brightest Cluster Sample (BCS; Ebeling et al. 1998, Table 2), and the dotted box corresponds to the extrapolation of the bright end of the ROSAT Deep Cluster Sample (RDCS) as given by Rosati et al. (1997).

Our best-fit to the LogN-LogS is systematically above that found for the BCS sample. The difference at a flux of  $3.05 \times 10^{-12} \text{ erg cm}^{-2} \text{ s}^{-1}$  is 19% and is significant at about the  $2\text{-}\sigma$  confidence level. Possible explanations of this difference could be the different efficiencies of the pre-selection methods used in compiling the two cluster samples or the different techniques used to estimate the X-ray fluxes.

Another sample of RASS1 clusters already available in the literature, and covering the sky at  $|b_{II}| > 20^\circ$ , is the X-ray Brightest Abell Cluster sample (XBACs; Ebeling et al. 1996). This sample, however, is optically-selected because it was compiled by looking for cluster soft X-ray emission over the objects in the Abell and ACO catalogs. Moreover the ROSAT energy band used to derive the X-ray fluxes was the broad band (0.1-2.4 keV).

In general our data are in good agreement with previ-

ous estimates of the LogN-LogS distribution, and moreover as both the EMSS and RDCS cluster samples are purely X-ray selected, the good agreement in the number counts suggests that our selection function, which is partially driven by the optical properties of clusters (see § 3), does not lead to a significant incompleteness.

## 6. COMPLETENESS OF THE RASS1 BRIGHT SAMPLE

In this section we discuss the possible sources of incompleteness in the RASS1 Bright Sample, which requires a review of the initial selection process of the RASS1 Candidate Sample.

### 6.1. Biases Introduced by the SASS1 Detection Algorithm and the SASS1 Count Rate Cut

As stated in § 3 the RASS1 Candidate Sample was selected from the SASS1 source list, and therefore one possible origin of incompleteness is related to limitations of the SASS1 in detecting and characterizing sources. The detection algorithm implemented within SASS1 was optimized to detect pointlike sources. Both the two sliding window and the ML techniques (see § 2.1) use fixed apertures to detect sources, so that extended sources with low surface brightness may either not be detected or have their count rates significantly underestimated. Another cause of underestimation of source count rates comes from the assumption made within the ML technique that the source brightness profile is a sum of Gaussians, which is not a good description of the profile of most galaxy clusters.

The conservative solution we adopted to effectively limit the incompleteness of the RASS1 Bright Sample with respect to extended sources, was to choose a very high limiting count rate. In the following, using the distribution of sources in Figure 4, we try to estimate the typical angular dimensions of the objects which may have been lost due to the effects described above. From Figure 4 we note that the more extended the source the further away it is from the bisector of the count rate plane (dot-dashed line), this is because the more extended sources suffer a severe underestimation of the count rate by SASS1. Therefore the sources which were missed in the RASS1 Bright Sample because they were not detected by SASS1, i.e. those which should fall in the top left quadrant in Figure 4, must be highly extended sources. We have seen that this incompleteness should be limited to  $\lesssim 5\%$  (§ 4.2.2). In order to estimate the typical extent of these clusters we have performed the following quantitative analysis on the data distribution reported in Figure 4. To first approximation, we can relate the distance of any straight line parallel to the one-to-one line with a value of the extension, i.e. the core radius. The sources which should fall in the top left quadrant in Figure 4, must have an extent larger than that corresponding to the straight line parallel to the bisector of the count rate plane crossing the point  $(cr_{SASS1}, cr_{SRT}) = (0.055, 0.25)$ . Drawing this line in Figure 4 we see that 11 sources fall above the line and that all these sources have a core radius larger than about 4 arcmin.

Therefore, the  $\sim 8.6$  sources that we estimated in § 4.2.2 to be probably missing from the sample because of the flux cuts, very probably have a core radius of 4 arcmin or larger. Taking a value for the physical core radius of 250 kpc and

a Hubble constant of  $50 \text{ km s}^{-1} \text{ Mpc}^{-1}$ , we calculate that a cluster with an angular core radius of 4 arcmin would have a redshift of 0.08. Thus the  $\sim 5\%$  incompleteness discussed in § 4.2.2 is most likely due to sources with redshifts smaller than  $\sim 0.08$ . This should be treated as a first order estimate, first because we have used an approximate analysis and second because clusters show a scatter in their physical core radii.

From a preliminary analysis of the ACO clusters within the area of the RASS1 Bright Sample (Böhringer et al. in preparation), we find that 6 ACO clusters with hard band count rate larger than 0.25 cts/s are missing from our sample. All but one of these clusters were detected from SASS1, but their SASS1 broad band count rates were  $< 0.055 \text{ cts/s}$ , i.e. below the initial SASS1 count rate limit of the RASS1 Candidate Sample. All these clusters have a measured redshift  $\lesssim 0.06$ , in agreement with our expectations about the bias against the more extended and nearby clusters and our completeness estimate of §4.2.2. The properties of these 6 ACO clusters are reported in Table 3.

<i>Column (1).</i>	— Name of the ACO cluster.
<i>Column (2).</i>	— Right ascension (J2000) in degrees.
<i>Column (3).</i>	— Declination (J2000) in degrees.
<i>Column (4).</i>	— SASS1 count rate measured in the (0.1-2.4 keV) band.
<i>Column (5).</i>	— measured redshift.
<i>Column (6).</i>	— redshift reference.

### 6.2. Biases Introduced by the Identification Process

As described in § 3, the RASS1 Candidate Sample was selected by basically two means of identification: the clusters were either found directly by their optical counterparts (overdensities in the COSMOS galaxy catalog – either direct or pre-processed –, or optical clusters in the Abell and ACO catalogs), or by having been flagged as extended sources during the SASS1 source analysis.

Clearly, this procedure is potentially prone to a number of selection effects, that can be summarized as follows.

1) *Optical counterparts.* The COSMOS galaxy catalog was produced through the analysis of digitized ESO/SRC J survey optical plates (Yentis et al. 1992), using automatic algorithms. One recognized problem of the digitization and star-galaxy separation processes is in the correct treatment of diffraction spikes and halos around bright stars and of the extended envelopes of cD galaxies (Heydon-Dumbleton et al. 1989). For our purposes, one can reasonably think that this effect will in general increase the contamination of the RASS1 Candidate Sample, by including spurious “clusters”, but should not reduce its completeness. A more serious concern is the misclassification of galaxies as stars, estimated to be around 5% in the COSMOS data. This could potentially reduce the contrast of a poor cluster and thus exclude it from the sample.

Concerning, on the other hand, the use of the Abell and ACO catalogs, one might worry that they are biased against poor systems (expected to be anyway rare in our sample, at  $z$  larger than  $\sim 0.04$ ), and are affected by subjective biases that are difficult to quantify a priori.

2) *X-ray extension.* Sources were classified as extended using the threshold values, extent radius larger than 25 arcsec and extent likelihood larger than 7 as supplied by

the ML algorithm of SASS1. This set of cuts has been used successfully before (for details see e.g. Fig. 7 in Ebeling et al. 1993). This method is however not reliable in recovering all extended sources, as we find directly that several very extended sources are not recognized.

To better understand the completeness of the global identification process within the selection limits of the RASS1 Bright Sample, we have tried to exploit the complementarity of these two methods. (Note that most of the clusters in the sample have been found by both methods).

Let us assume that the two means of identification are uncorrelated, which is the case if clusters are missed by simple independent errors in the two techniques. This allows us to statistically infer the incompleteness of the sample in the following way. We define by  $O$  the set of clusters found by optical means and by  $X$  the set found by X-ray extent.

The statistical independence of the two search methods, allows us to write the combined probability of events  $O$  and  $X$ , as

$$P(O \cap X) = P(O) \cdot P(X). \quad (4)$$

Defining  $T$  as the parent sample (i.e.,  $P(T) \equiv 1$ ), we can relate probabilities,  $P$ , to occurrences,  $N$ , in the following way:  $P(X) = N(X)/N(T)$ ,  $P(O) = N(O)/N(T)$  and  $P(O \cap X) = N(O \cap X)/N(T)$ . Substituting in equation (4) we obtain:

$$N(T) = \frac{N(O) N(X)}{N(O \cap X)}, \quad (5)$$

and using the actual numbers in the subsets,  $N(O) = 118$ ,  $N(X) = 95$ , and  $N(O \cap X) = 83$ , we find  $N(T) = 135$ . Consequently, the missing fraction of objects for our 130 clusters sample is  $\sim 3.7\%$ .

The assumption that the two methods of detection are uncorrelated is probably not strictly valid, as poor and more distant clusters will be harder to find for both techniques. Therefore the number calculated for the clusters missed is a lower limit to the missing fraction, but it is already reassuring that this fraction is as low as 3.7%.

### 6.3. $\langle V/V_{max} \rangle$ Test

As a final check, we have tested the spatial distribution of the bright clusters with the  $V/V_{max}$  method. Since our sample has different flux limits (§ 5.2) we have used the generalization of the  $V/V_{max}$  method (Schmidt 1968) given in Avni & Bahcall (1980). We have also assumed an Einstein-deSitter cosmological model with  $\Lambda = 0$ ,  $q_0 = 0.5$  and  $H_0 = 50 \text{ km s}^{-1} \text{ Mpc}^{-1}$ . The derived  $\langle V/V_{max} \rangle$  is  $0.49 \pm 0.16$ , consistent with uniformity.

## 7. SUMMARY AND CONCLUSIONS

The aim of the present work was to derive an X-ray flux limited sample of bright clusters of galaxies characterized by a high degree of completeness. It is based on a first cluster candidate sample derived in the ESOKP collaboration, belonging to the southern Galactic cap region ( $\delta < 2.5^\circ$  and  $b_{II} < -20^\circ$ ). This is called in our paper the RASS1 Candidate Sample and contains 679 sources.



We performed first a detailed reanalysis of fluxes for all sources in this RASS1 Candidate Sample by using the RASS merged data and the SRT method developed and discussed in Paper I.

We have applied to the RASS1 Candidate Sample various restrictive selections aimed at heavily reducing the sources of incompleteness. Our first selection set a lower limit of 150 s to the exposure time in order to avoid regions of sky where objects could have been missed because of the low sensitivity of the survey. In the second selection we excluded crowded regions of the sky, i.e. the Galactic plane and the Magellanic Clouds, to avoid confusion problems affecting optical and X-ray catalogs. The third selection set a lower limit to the SRT count rate of 0.25 cts/s in the hard band. In setting the SRT count rate limit, we investigated the behavior of a control sample of optically identified objects, namely the EMSS sample reobserved in the RASS. These selections yielded an X-ray completeness in the derived sample of  $\sim 95\%$ . Such a high degree of completeness was reached at the expenses of reducing drastically the number of candidates in our sample, from 679 to 164.

We used our new data from the ESOKP, together with data drawn from the literature to identify the selected candidates. After removing a number of false identifications we produced a sample which contains 130 clusters with X-ray fluxes larger than  $\sim 3.5 \times 10^{-12}$  erg cm $^{-2}$  s $^{-1}$  and  $z \lesssim 0.3$ , covering a sky area of 8235 deg $^2$ .

We have then investigated the various sources of incompleteness and biases, which could be affecting the RASS1 Bright sample. The key factor allowing us to constrain the incompleteness has been to apply a cut at a relatively high X-ray count rate. This action limits the bias against very extended X-ray sources (i.e. nearby clusters and groups). From our estimates we have also seen that this bias is kept under control for redshifts  $\lesssim 0.08$  and eliminated for red-

shifts  $\gtrsim 0.08$ .

A statistical estimate of the completeness level of the identification procedure, based on the relative success rates of the two main methods of cluster identification (optical-vs. X-ray-based), indicates an incompleteness  $\sim 4\%$  due to this source. Adding this to that estimated from the flux selection procedure, we obtain a global completeness for the sample which is better than 90%.

The LogN-LogS distribution is well described by a power law with slope  $\alpha = 1.34 \pm 0.15$  and normalization  $A = 11.87 \pm 1.04$  sr $^{-1}(10^{-11}$  erg cm $^{-2}$  s $^{-1})^\alpha$ . A comparison between our result and previous measurements shows good agreement.

The sample discussed here should represent a useful database for a number of statistical studies on the properties of clusters of galaxies in the local Universe. Finally, we should mention that the results presented here will be extended by the future developments of the ongoing ESOKP collaboration.

The authors would like to thank the ROSAT team at MPE. H. T. MacGillivray at ROE and D. J. Yentis at NRL for having provided the COSMOS digitized optical sky survey catalogs. We thank also K. Romer for having allowed us to publish eight redshifts from the SGP project and J. P. Henry and C. R. Mullis for having provided two new redshifts. SDG would like to thank P. Rosati, R. Della Ceca and G. Zamorani for useful comments and discussions. Special thanks also to C. Izzo at MPE for his help in the data analysis. This research has made use of data provided by the NED and the SIMBAD databases and by the digitized optical images from the POSS and UK Schmidt sky surveys obtained through the SKYVIEW facility. We also used data from the HEASARC online service and the ROSAT public archive. We thank all those who contribute in maintaining these databases.

## REFERENCES

- Abell, G. O., Corwin, H. G., Olowin, R. P. 1989, ApJS, 70, 1  
 Allen, S. W., Edge, A. C., Fabian, A. C., Böhringer, H., Crawford, C. S., Ebeling, H., Johnstone, R. M., Naylor, T., Schwarz, R. A. 1992, MNRAS, 259, 67  
 Avni, Y. & Bahcall, J.N., 1980, ApJ, 235, 694  
 Bahcall, N.A., 1975, ApJ, 198, 249  
 Bahcall, N.A. & Cen, R. 1993, ApJ, 407, L49  
 Böhringer, H. 1994, in Studying the Universe with Clusters of Galaxies, Böhringer H. & Schindler S. (eds), MPE report 256, 93  
 Böhringer, H. 1995, in the Proc. of the Texas Symp. on Relativistic Astrophysics and Cosmology, H. Böhringer, J. Trümper, and G. E. Morfill (eds.), Annals of the New York Academy of Science, Vol. 759, 67  
 Böhringer, H. et al. 1998, in the Proc. of XIII IAP Meeting "Wide-Fields Surveys", S. Colombi & Mellier (eds.), Paris, in press  
 Briel, U. G. & Pfeffermann, E. 1986, Nucl. Instr. and Methods, A242, 376  
 Briel, U. G. & Henry, J. P. 1993, A&A, 278, 379  
 Brinkmann, W., Siebert, J. & Böller, T. 1994, A&A, 281, 355  
 Burg, R., Giacconi, R., Huchra, J., MacKenty, J., Mclean, B., Geller, M., Hasinger, G., Marzke, R., Schmidt, M. & Trümper, J. 1992, A&A, 259, L9  
 Collins, C. A., Guzzo, L., Nichol, R. C., Lumsden, S. L. 1995, MNRAS, 274, 1071  
 Collins, C.A., Nichol, R.C., Romer, A.K., & Burke, A., 1997, ApJ, 479, L117  
 Crawford, D. F., Jauncey, D. L. & Murdoch, H. S. 1970, ApJ, 162, 405  
 Crawford, C. S., Edge, A. C., Fabian, A. C., Allen, S. W., Böhringer, H., Ebeling, H., McMahon, R. G., Voges, W. 1995, MNRAS, 274, 75  
 Cruddace, R. G., Hasinger, G. R., Schmitt, J. H. 1988, in Astronomy from Large Database, F. Murtagh & A. Heck (eds), 177  
 Dalton, G. B., Efstathiou, G., Maddox, S. J., Sutherland, W. J. 1994, MNRAS, 269, 151  
 Dalton, G. B., Maddox, S. J., Sutherland, W. J., Efstathiou, G., 1997, MNRAS, 289, 263  
 De Grandi, S. 1996a, PhD-Thesis, University of Milan  
 De Grandi, S. 1996b, in MPE Rep. 263, Proc. Röntgenstrahlung from the Universe, ed. H. U. Zimmerman, J. Trümper, & H. Yorke (Munich: MPE), 577  
 De Grandi, S., Molendi, S., Böhringer, H., Chincarini, G. & Voges, W. 1997, ApJ, 486, 738  
 De Grandi, S., Guzzo, L., Böhringer, H., Molendi, S., Collins, C., Cruddace, R., Neumann, D., Schindler, S., Schuecker, P. and Voges, W. 1999, ApJ, in press  
 den Hartog, R. & Katgert, P. 1996, MNRAS, 279, 349  
 de Vaucouleurs, G., de Vaucouleurs, A., Corwin Jr., H. G., Buta, R. J., Paturel, G. & Fouque, P. 1991, Third Reference Catalog of Bright Galaxies, version 3.9  
 Dickey, J. M. & Lockman, F. J. 1990, Ann. Rev. Astron. Astroph., 28, 215  
 Douglas, J. N., Bash, F. N., Bozyan, F. A., Torrence, G. W. & Wolfe, C. 1996, AJ, 111, 1945  
 Ebeling, H., Voges, W., Böhringer, H., Edge, A. C. 1993, A&A, 275, 360  
 Ebeling, H. & Maddox, S. J. 1995, MNRAS, 275, 1155  
 Ebeling, H., Voges, W., Böhringer, H., Edge, A. C., Huchra, J. P., Briel, U. G. 1996, MNRAS, 281, 799  
 Ebeling, H., Edge, A.C., Fabian, A.C., Allen, S. W., Crawford, C. S. & Böhringer, H., 1997, ApJ, 479, 101  
 Ebeling, H., Edge, A.C., Böhringer, H., Allen, S.W., Crawford, C.S., Fabian, A.C., Voges, W., Huchra, J.P. 1998, MNRAS, 301, 881

- Evrard, A. E. 1997, MNRAS, 292, 289
- Frenk, C.S., White, S.D.M., Efstathiou, G. & Davis, M. 1990, ApJ, 351, 10
- Galli, M., Cappi, A., Focardi, P., Gregorini, L., Vettolani, G. 1993, A&AS, 101, 259
- Garcia, A. M. 1993, A&A, 100, 47
- Gawiser, E. & Silk, J. 1998, Science, 280, 1405
- Gioia, I. M., Henry, J. P., Maccacaro, T., Morris, S. L., Stocke, J. T., and Wolter, A. 1990, ApJ, 356, 35
- Gioia, I. M. & Luppino, G. A. 1994 ApJS, 94, 583
- Guzzo, L. et al. 1995, in Wide Field Spectroscopy and Distant Universe, Maddox S. J. & Aragon-Salamanca A. (eds), World Scientific, 205
- Heydon-Dumbleton, N. H., Collins, C. A. & MacGillivray, H. T. 1989, MNRAS, 238, 379
- Henry, J. P., Gioia, I. M., Maccacaro, T., Morris, S. L., Stocke, J. T., & Wolter, A. 1992, ApJ, 386, 408
- Huchra, J., Latham, D. W., Da Costa, L. N., Pellegrini, P. S., Willmer, C. N. A. 1993, AJ, 105, 1637
- Jones et al., 1998, ApJ, 495, 100
- Jones, C. & Forman, W., 1984, ApJ, 276, 38
- King, I.R. 1966, AJ, 71, 64
- Kitayama, T., & Suto, Y. 1997, ApJ, 490, 557
- Lauberts, A. & Valentijn, E. A. 1989, The Surface Photometry Catalog of the ESO-Uppsala Galaxies, Garching bei Munchen: European Southern Observatory
- Ledlow, M. J. & Owen, F. N. 1995, AJ, 109, 853
- Mazure, A., Katgert, P., den Hartog, R., Biviano, A., Bubath, P., Escalera, E., Focardi, P., Gerbal, D., Giuricin, G., Jones, B., Le Fevre, O., Moles, M., Perea, J., Rhee, G. 1996, A&A, 310, 31
- Maccacaro, T., Gioia, I. M., Wolter, A., Zamorani, G. & Stocke, J. T. 1988, ApJ, 326, 680
- Maccacaro, T., Wolter, A., McLean, B., Gioia, I. M., Stocke, J. T., Della Ceca, R., Burg, R., and Faccini, R. 1994, Astro Lett. and Communications, 29, 267
- Murdoch, H. S., Crawford, D. F. & Jauncey, D. L. 1973, ApJ, 183, 1
- Muriel, H., Nicotra, M. A., & Lambas, D. 1990, AJ, 100, 339
- Muriel, H., Nicotra, M. A., & Lambas, D. 1995, AJ, 110, 1032
- NED11 1992, Redshift Obtained from Literature by the NED Team prior to November 1992, vol. Report p.1
- Piccinotti, G., Mushotzky, R. F., Boldt, E. A., Holt, S. S., Marshall, F. E., Serlemitsos, P. J., & Shafer, R. A. 1982, ApJ, 253, 485
- Postman, M. & Lauer, T. 1995, ApJ, 440, 28
- Postman, M., Huchra, J. P. & Geller, M. J. 1992 ApJ, 384, 404
- Quintana, H. & Ramirez, A. 1995, ApJS, 96, 343
- Romer, A. K., Collins, C. A., Böhringer, H., Cruddace, R. G., Ebeling, H., MacGillivray, H. T. & Voges, W. 1994, Nature, 372, 75
- Rosati, P., Della Ceca, R., Burg, R., Norman, C. & Giacconi, R. 1995, ApJ, 445, 11
- Rosati, P., Della Ceca, R., Norman, C. & Giacconi, R. 1997, ApJL, 492, 21
- Sarazin, C. L. 1988, X-ray Emission from Clusters of Galaxies (Cambridge Univ. Press: Cambridge)
- Schmidt, M., 1968, ApJ, 151, 393
- Snowden, S. L. & Petre, R. 1994, ApJ, 436, L123
- Stocke, J. T., Morris, S. L., Gioia, I. M., Maccacaro, T., Schild, R., Wolter, A., Fleming, T. A., Henry, J. P. 1991 ApJS, 76, 813
- Struble, M. F. & Rood, H. J. 1987, ApJS, 63, 543
- Struble, M. F. & Rood, H. J. 1991, ApJ, 374, 395
- Teague, P. F., Carter, D., Gray, P. M. 1990, ApJS, 72, 1715
- Trümper, J. 1993, Science, 260, 1769
- Tucker, W. H., Tananbaum, H. & Remillard, R. A., 1995, AJ, 444, 532
- Voges, W. 1992, in Proceedings of Satellite Symposium 3, ed. T. D. Guyenne & J. J. Hunt, ESA-ESY-3 (Noordwijk:ESA), 9
- White, S.D.M., Efstathiou, G. & Frenk, C.S. 1993, MNRAS, 262, 1023
- Yentis, D. J., Cruddace, R. G., Gursky, H., Sturat, B. V., et al. 1992, in the Proc. of Digitized Optical Sky Surveys, H. T. MacGillivray & E. B. Thompson (eds.), Kluwer Academic Publ., 67
- Zabludoff, A. I., Geller, M. J., Huchra, J. P., Vogeley, M. S. 1993, AJ, 106, 1273
- Zimmermann, H. U., Boese, G., Becker, W., Belloni, T., Döbereiner, S., Izzo, C., Kahabka, P. & Schwentker, O. 1997, EXSAS User's Guide, <http://wave.xray.mpe.mpg.de/users-guide>

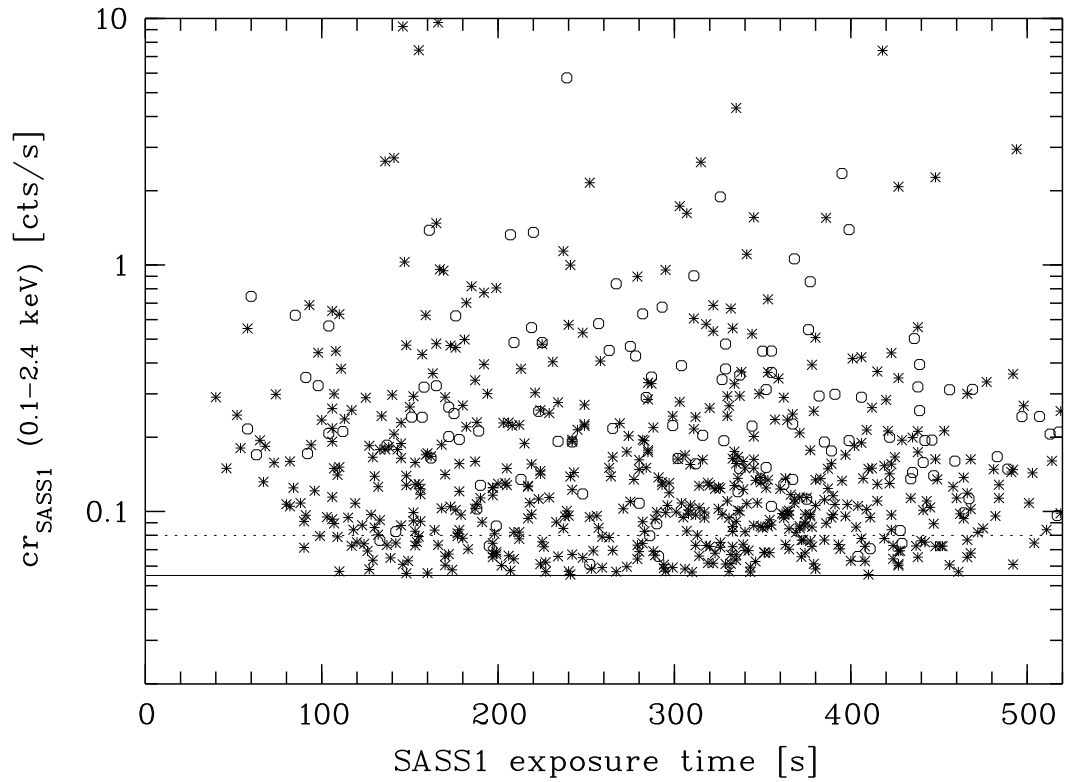


FIG. 1.— SASS1 broad band count rates versus SASS1 exposure times for the RASS1 Candidate Sample. Sources which were found to be pointlike with the SRT are indicated as asterisks, while sources which were found to be extended are indicated as open circles. The dotted and solid lines represent the limiting SASS1 count rates 0.08 and 0.055 cts/s, respectively.

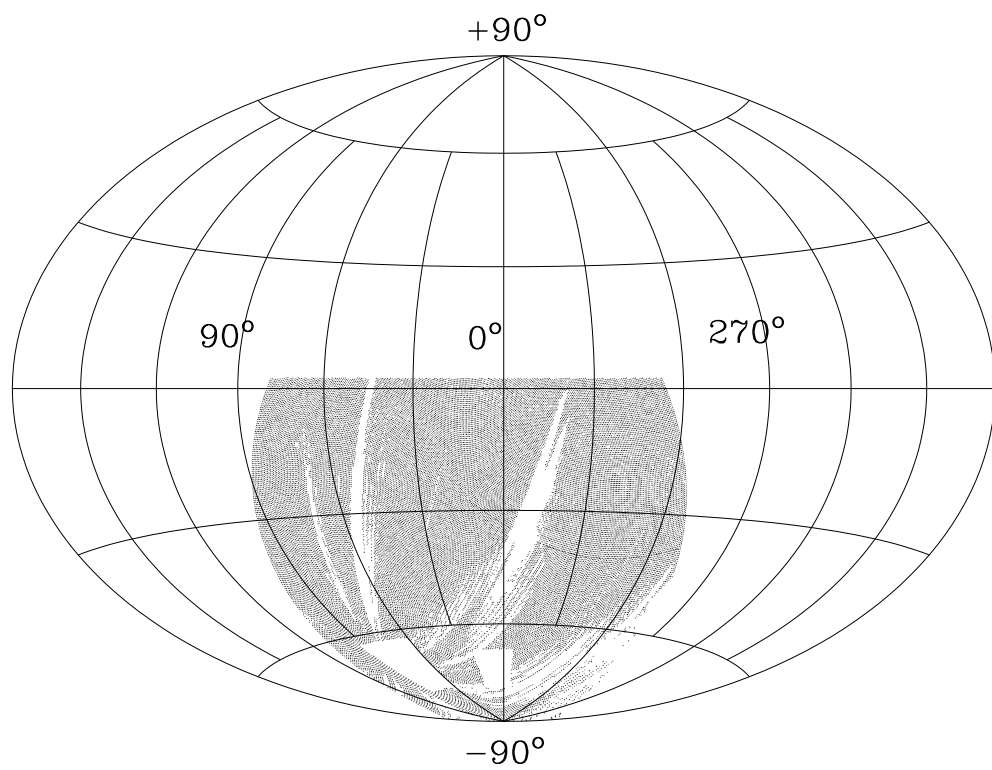


FIG. 2.— Total sky area covered by the RASS1 Bright Sample in equatorial coordinates (J2000.0). Regions with low exposure times ( $< 150$  s) and the Magellanic Clouds are shown in white.

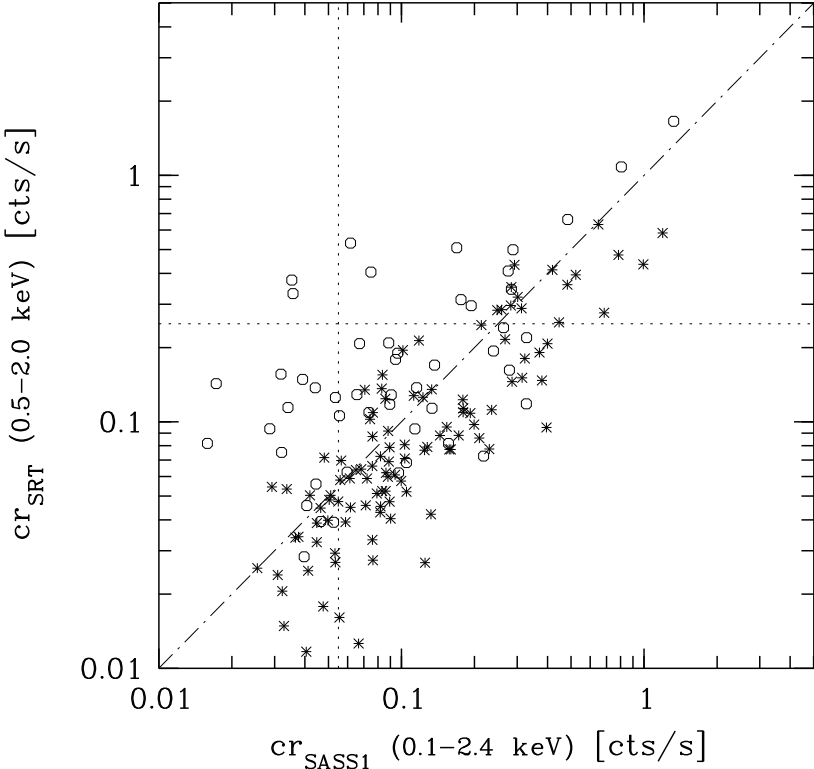


FIG. 3.— SRT hard band count rates versus SASS1 broad band count rates for the EMSS control sample. Asterisks indicate pointlike objects (i.e. AGNs and stars), open circles indicate potentially extended sources (i.e. galaxies and galaxy clusters). The vertical and horizontal dotted lines represent the SASS1 count rate limit, 0.055 cts/s, and the SRT count rate limit, 0.25 cts/s, respectively. The dot-dashed line indicates the bisector of the count rate plane.

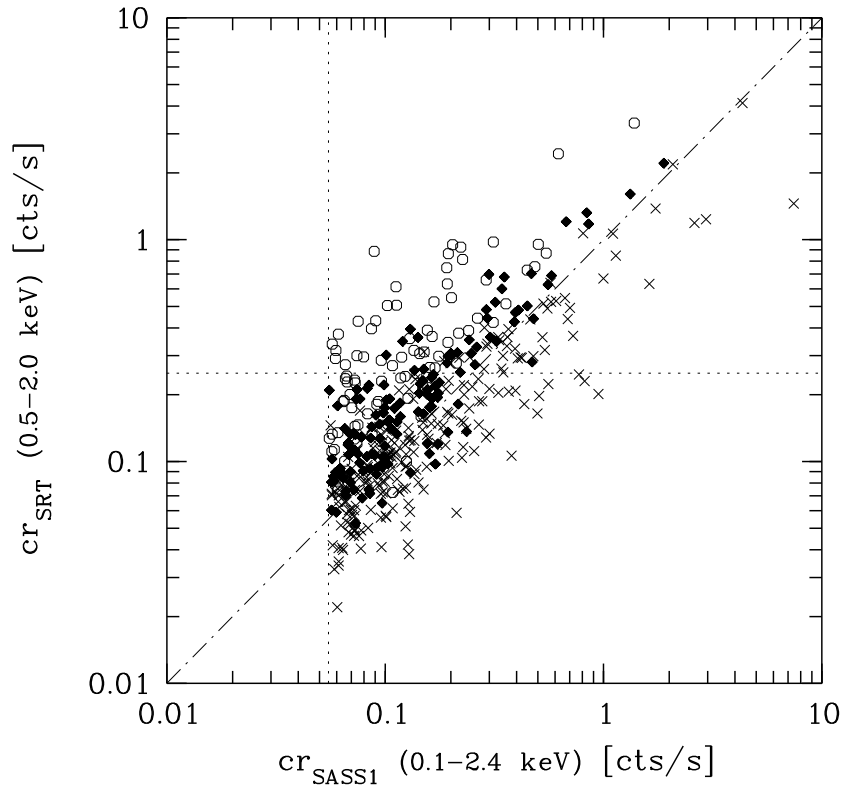


FIG. 4.— SRT hard band count rates versus SASS1 broad band count rates for the SUB1 cluster candidate sample (see § 4.2.2 for definition). Crosses correspond to sources with core radii  $< 1$  arcmin, filled squares to sources with core radii from 1 to 2 arcmin, and open circles to sources with core radii  $> 2$  arcmin. The vertical and horizontal dotted lines represent the SASS1 count rate limit, 0.055 cts/s, and the SRT count rate limit, 0.25 cts/s, respectively.

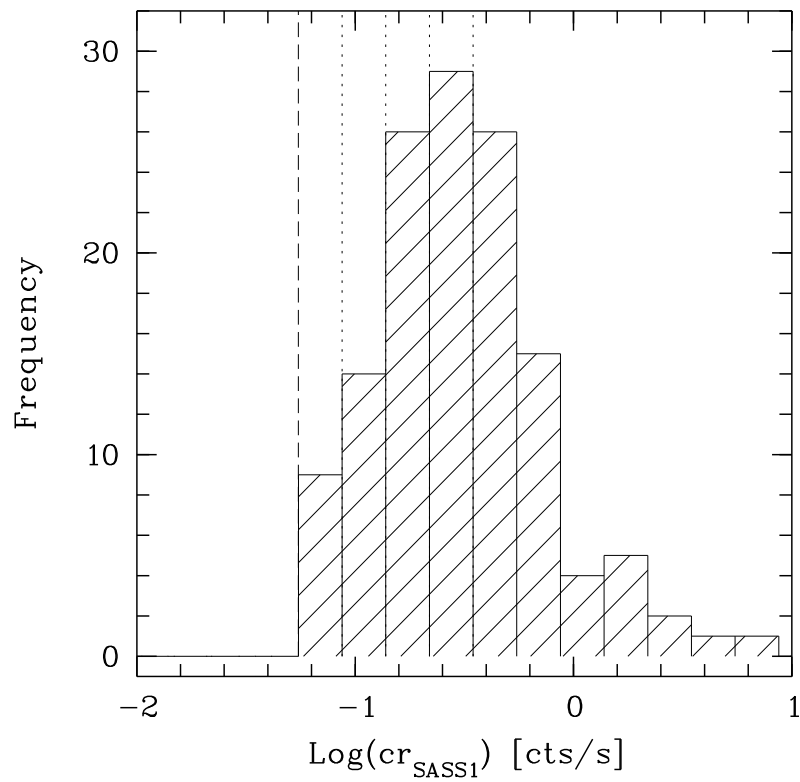


FIG. 5.— SASS1 broad band count rates of SUB1 sources with an SRT hard band count rates  $> 0.25$  cts/s. The long dashed line is the SASS1 count rate limit of 0.055 cts/s, the dotted lines show the bins used for the fit (see text for details).

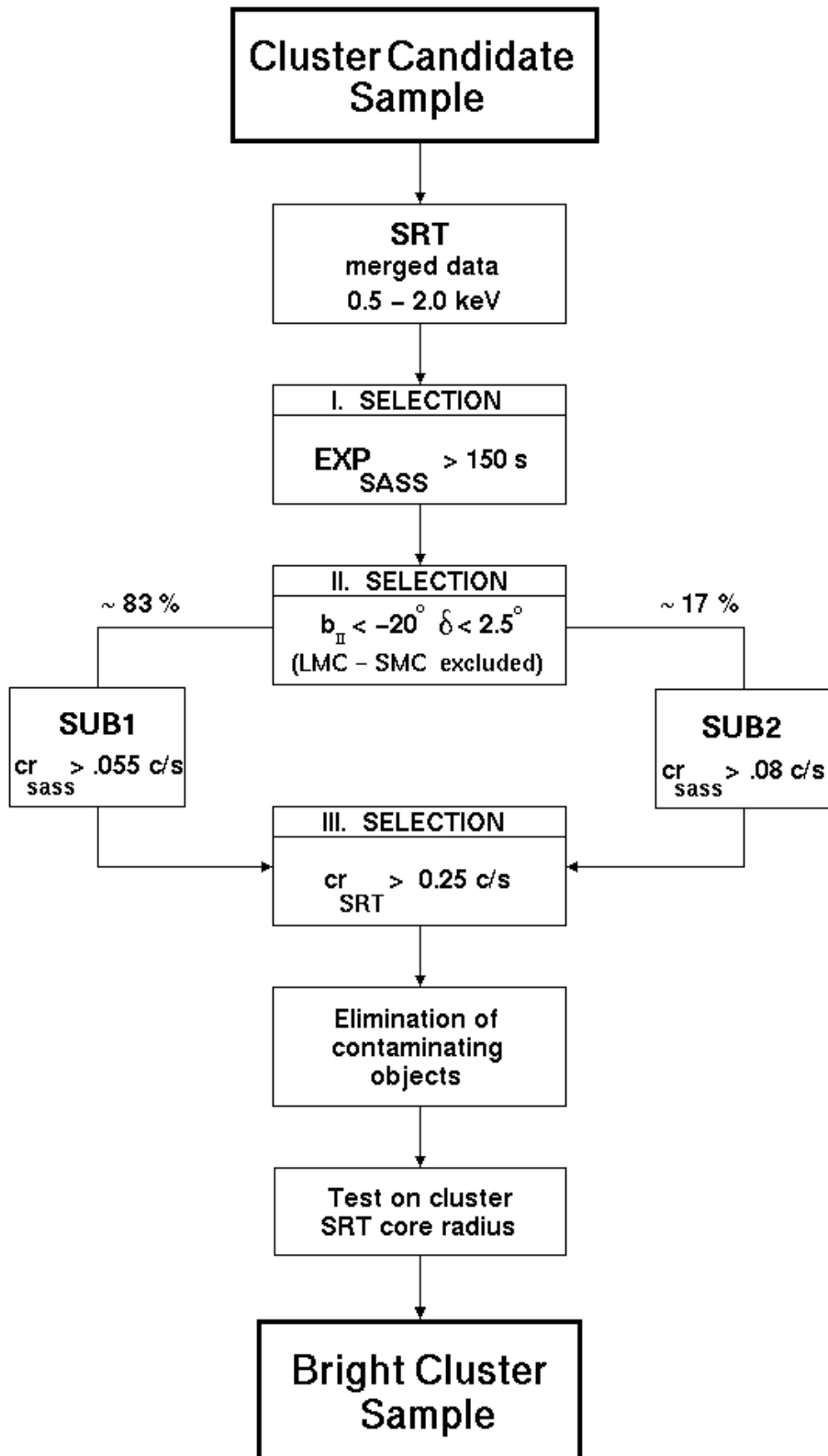


FIG. 6.— Schematic representation of the selections applied to the RASS1 Candidate Sample to obtain the RASS1 Bright Sample.



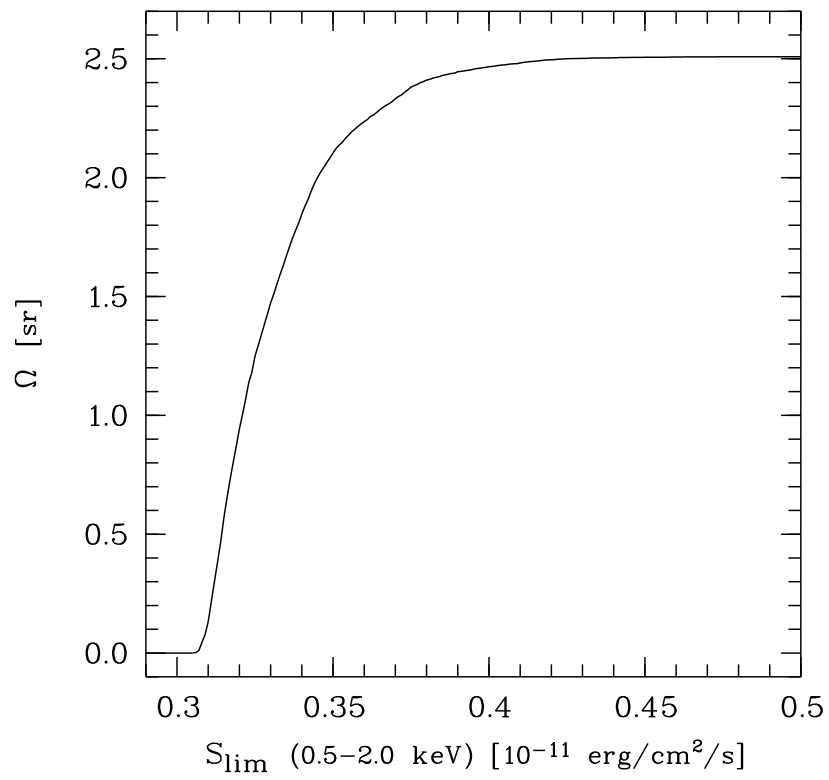


FIG. 7.— Sky coverage as a function of the flux limit for the RASS1 Bright Sample.

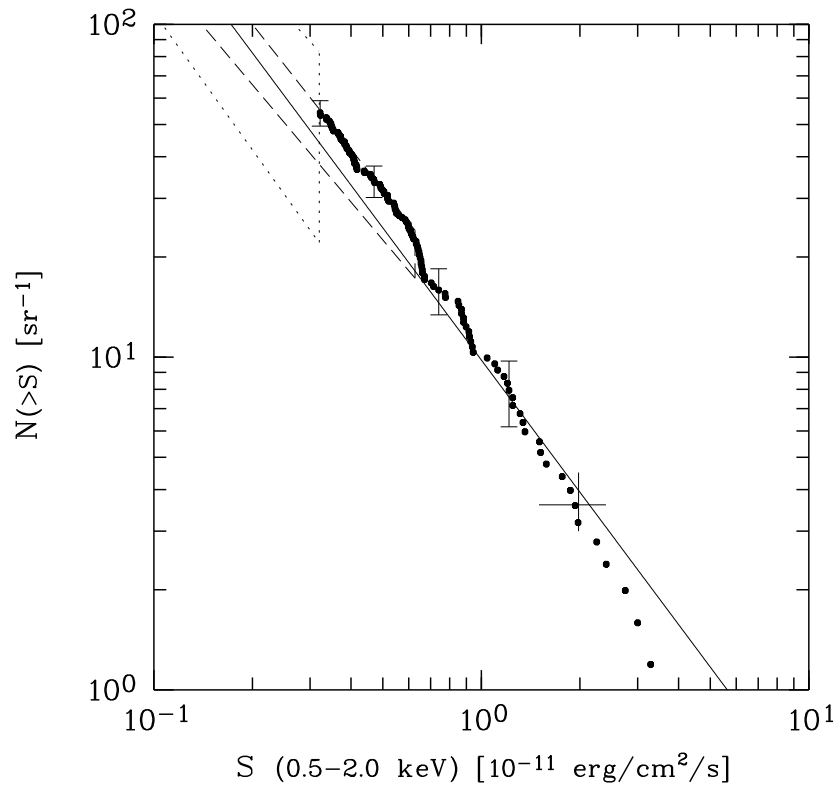


FIG. 8.— Cumulative cluster number counts distribution, LogN-LogS, of the RASS1 Bright Sample (dots). Vertical error bars on a few individual points represent the uncertainty in the number of clusters. Also shown for comparison are the LogN-LogS of other cluster samples: the long-dashed box represents the EMSS LogN-LogS (Henry et al. 1992) as recalculated in Rosati et al. (1995), the cross represents the Piccinotti et al. (1982) point, the dotted box is the extrapolation of the bright end of the RDCS sample by Rosati et al. (1997), and the solid line represents the best-fit of the BCS sample (Ebeling et al. 1998).

TABLE 1  
CLUSTER CATALOG

Sequence	RA(J2000) Dec(J2000)	NH	Time	cr(5') Err	cr(SRT) Err $\pm$	P	F <sub>X</sub> Err	L <sub>X</sub> Err	ID Class	z Ref	Note
(1)	(2)	(3)	(4)	(5)	(6)	(7)	(8)	(9)	(10)	(11)	(12)
001	00 03 09.41 −35 56 22.0	1.09	335.7	0.26 0.03	0.51 +0.13 −0.10	9.9e−04	0.62 0.14	0.64 0.15	A2717 A	0.0490 (1)	
002	00 05 59.39 −34 43 05.5	1.16	348.4	0.20 0.03	0.27 +0.05 −0.05	4.0e−02	0.34 0.06	1.86 0.33	A2721 A	0.1140 (2)	
003	00 11 20.51 −28 51 05.0	1.84	329.5	0.40 0.04	0.70 +0.12 −0.11	3.6e−04	0.88 0.14	1.44 0.23	A2734 A	0.0617 (1)	
004	00 13 37.12 −19 29 54.0	2.00	318.1	0.22 0.03	0.30 +0.05 −0.05	4.9e−02	0.37 0.06	1.41 0.24	A0013 A	0.0943 (1)	
005	00 14 20.32 −30 22 58.0	1.65	332.2	0.23 0.03	0.28 +0.04 −0.04	1.1e−01	0.35 0.05	13.97 2.16	A2744 A	0.3080 (2)	
006	00 20 44.05 −25 42 21.0	2.26	318.7	0.21 0.03	0.33 +0.07 −0.06	1.5e−02	0.42 0.08	3.62 0.72	A0022 A	0.1432 (3)	
007	00 25 34.36 −33 02 43.0	1.69	337.8	0.29 0.03	0.51 +0.11 −0.09	1.1e−03	0.64 0.12	0.68 0.13	S0041 A	0.0498 (2)	
008	00 28 35.89 −23 39 07.0	1.82	313.2	0.21 0.03	0.39 +0.12 −0.09	4.1e−03	0.49 0.13	2.46 0.65	A0042 A	0.1087 (4)	
009	00 41 50.11 −09 18 17.5	3.58	385.8	1.89 0.07	3.11 +0.19 −0.19	3.6e−07	4.09 0.25	5.41 0.33	A0085 A	0.0556 (1)	
010	00 42 08.63 −28 32 09.0	1.49	336.0	0.41 0.04	0.49 +0.05 −0.05	1.2e−01	0.61 0.07	3.06 0.33	A2811 A	0.1087 (5)	
011	00 49 24.05 −29 31 21.0	1.80	331.5	0.19 0.03	0.26 +0.05 −0.05	5.2e−02	0.32 0.06	1.66 0.32	S0084 A	0.1100 (2)	
012	00 52 34.76 −80 15 21.0	6.64	252.2	0.30 0.04	0.36 +0.06 −0.05	1.5e−01	0.52 0.08	2.87 0.43	A2837 A	0.1142 (6)	
013	00 56 11.69 −01 14 52.5	3.10	295.6	0.43 0.04	1.85 +0.66 −0.55	1.8e−06	2.41 5.16	2.90 4.32	A0119 A	0.0442 (1)	
014	01 02 42.21 −21 52 43.5	1.60	361.5	0.73 0.05	1.27 +0.15 −0.13	1.7e−05	1.58 0.17	2.16 0.24	A0133 A	0.0566 (1)	
015	01 07 49.61 −36 43 43.5	1.86	388.3	0.16 0.02	0.30 +0.09 −0.07	6.4e−03	0.37 0.10	2.35 0.64	A2871 A	0.1219 (1)	
016	01 08 13.14 −02 11 33.0	3.01	434.8	0.14 0.02	0.40 +0.25 −0.13	1.5e−03	0.52 0.26	0.42 0.21	A0147 A	0.0438 (4)	
017	01 08 52.89 −15 25 45.5	1.69	460.2	0.25 0.02	0.51 +0.11 −0.09	1.9e−04	0.63 0.13	0.77 0.16	A0151 A	0.0533 (1)	
018	01 09 52.59 −45 55 42.0	2.10	310.9	0.21 0.03	0.39 +0.11 −0.09	4.4e−03	0.49 0.13	0.12 0.03	A2877 A	0.0241 (2)	
019	01 14 59.52 −00 22 13.9	3.32	434.5	0.17 0.02	0.71 +0.26 −0.22	2.6e−04	0.93 2.23	0.97 1.92	A0168 A	0.0448 (7)	
020	01 20 58.78 −13 51 07.0	1.85	293.7	0.39 0.04	0.73 +0.14 −0.12	3.1e−04	0.92 0.17	1.03 0.19	0118.5-1408 A	0.0511 (8)	1
021	01 25 29.89 −01 45 40.0	3.08	435.1	0.19 0.02	0.30 +0.06 −0.05	7.0e−03	0.39 0.07	0.05 0.01	NGC0533 A	0.0171 (6)	2

TABLE 1—*Continued*

Sequence	RA(J2000) Dec(J2000)	NH	Time	cr(5') Err	cr(SRT) Err $\pm$	P	F <sub>X</sub> Err	L <sub>X</sub> Err	ID Class	z Ref	Note
(1)	(2)	(3)	(4)	(5)	(6)	(7)	(8)	(9)	(10)	(11)	(12)
022	01 31 52.69 −13 36 38.0	1.56	466.4	0.24 0.02	0.33 +0.05 −0.05	1.2e−02	0.42 0.06	7.43 1.06	A0209 A	0.2060 (4)	
023	01 37 16.19 −09 11 40.0	2.75	456.7	0.26 0.03	0.51 +0.11 −0.09	1.7e−04	0.66 0.13	0.44 0.08	... A	0.0392 (8)	3
024	01 45 07.63 −53 01 58.5	2.35	251.2	0.22 0.03	0.43 +0.09 −0.09	5.0e−03	0.55 0.17	3.35 1.03	A2941 A	0.1183 (6)	
025	02 25 52.81 −41 54 46.0	2.14	409.3	0.18 0.02	0.28 +0.04 −0.04	7.7e−03	0.35 0.08	7.43 1.53	A3017 A	0.2195 (8)	4
026	02 31 56.22 −01 14 59.5	2.89	256.0	0.08 0.02	0.29 +2.24 −0.17	2.3e−02	0.38 2.05	0.08 0.43	UGC02005 C	0.0221 (8)	5
027	02 32 18.69 −44 20 41.5	2.61	388.8	0.22 0.03	0.31 +0.05 −0.05	2.0e−02	0.40 0.07	13.29 2.17	... A	0.2836 (8)	6
028	02 49 36.03 −31 11 09.5	1.80	430.7	0.23 0.02	0.37 +0.06 −0.06	4.1e−03	0.46 0.08	0.10 0.02	S0301 A	0.0223 (2)	
029	03 03 24.17 −01 56 03.5	7.82	259.7	0.18 0.03	0.26 +0.06 −0.06	4.5e−02	0.38 0.09	3.79 0.85	A0409 A	0.1530 (9)	
030	03 07 03.50 −28 40 01.5	1.36	254.3	0.18 0.03	0.26 +0.05 −0.05	2.9e−02	0.32 0.09	9.15 2.31	A3088 A	0.2534 (6)	
031	03 14 22.59 −45 25 10.5	3.57	345.7	0.29 0.03	0.46 +0.08 −0.07	3.7e−03	0.60 0.10	1.32 0.22	A3104 A	0.0718 (6)	
032	03 17 58.85 −44 14 07.0	2.53	513.0	1.07 0.05	1.38 +0.08 −0.08	1.5e−02	1.77 0.10	4.24 0.24	A3112 A	0.0750 (1)	
033	03 28 37.24 −55 42 27.5	3.09	559.7	0.31 0.02	0.44 +0.05 −0.05	5.9e−03	0.57 0.06	1.79 0.20	A3126 A	0.0856 (1)	
034	03 30 01.11 −52 35 39.5	1.47	764.1	0.22 0.02	0.44 +0.08 −0.07	2.2e−05	0.55 0.09	0.72 0.12	A3128 A	0.0554 (2)	7
035	03 42 53.06 −53 37 43.0	1.06	702.9	0.89 0.04	1.83 +0.17 −0.15	1.6e−11	2.25 0.20	3.36 0.29	A3158 A	0.0591 (1)	
036	03 45 58.30 −24 16 45.0	1.58	484.2	0.21 0.02	0.35 +0.07 −0.06	2.0e−03	0.44 0.08	2.07 0.36	A0458 A	0.1050 (4)	
037	03 51 25.86 −82 12 44.5	7.65	368.0	0.31 0.03	0.85 +0.32 −0.21	3.2e−05	1.25 0.40	2.00 0.64	S0405 A	0.0613 (6)	
038	03 52 25.09 −74 01 02.5	8.02	766.9	0.38 0.02	0.71 +0.12 −0.11	4.0e−07	1.04 0.14	7.62 0.96	A3186 A	0.1270 (10)	
039	04 13 59.19 −38 05 50.0	1.41	481.8	0.42 0.03	0.63 +0.07 −0.07	1.5e−03	0.78 0.08	0.84 0.09	1ES0412-382 A	0.0502 (6)	8
040	04 19 39.01 −02 24 24.5	11.5	291.5	0.73 0.05	1.20 +0.14 −0.13	1.3e−04	1.93 0.22	0.13 0.01	NGC1550 B	0.0123 (11)	9
041	04 25 51.02 −08 33 38.5	6.40	272.7	0.88 0.06	1.32 +0.13 −0.13	7.2e−04	1.87 0.18	1.26 0.12	EXO0422-086 A	0.0397 (6)	
042	04 30 58.82	1.48	1460.6	0.75	2.42	1.3e−33	3.00	9.53	A3266	0.0589	

TABLE 1—*Continued*

Sequence	RA(J2000) Dec(J2000)	NH	Time	cr(5') Err	cr(SRT) Err $\pm$	P	F <sub>X</sub> Err	L <sub>X</sub> Err	ID Class	z Ref	Note
(1)	(2)	(3)	(4)	(5)	(6)	(7)	(8)	(9)	(10)	(11)	(12)
	−61 27 52.5			0.02	+0.70 −0.58		1.92	2.85	A	(1)	
043	04 33 37.07 −13 15 20.0	5.68	251.1	1.82 0.09	3.35 +0.31 −0.28	6.9e−08	4.65 0.41	2.15 0.19	A0496 A	0.0328 (7)	
044	04 45 11.28 −15 51 14.0	4.78	492.3	0.19 0.02	0.65 +0.42 −0.22	9.6e−05	0.88 0.46	0.50 0.26	NGC1650 B	0.0363 (12)	10
045	05 00 43.81 −38 40 25.5	3.07	456.0	0.18 0.02	0.50 +0.25 −0.15	3.2e−04	0.65 0.26	0.80 0.33	A3301 A	0.0536 (1)	
046	05 10 43.85 −08 01 13.0	8.30	406.3	0.22 0.03	0.31 +0.05 −0.05	2.4e−02	0.46 0.07	9.30 1.47	... A	0.2195 (6)	
047	05 25 32.56 −31 36 13.5	1.75	517.0	0.31 0.03	0.54 +0.08 −0.07	2.5e−04	0.67 0.10	0.41 0.06	A3341 A	0.0378 (1)	
048	05 28 55.06 −39 27 54.0	2.10	638.2	0.24 0.02	0.30 +0.03 −0.03	1.1e−01	0.37 0.04	12.54 1.33	... A	0.2839 (6)	11
049	05 30 35.81 −22 27 56.0	2.57	367.9	0.16 0.02	0.27 +0.05 −0.05	3.9e−03	0.34 0.13	5.49 1.65	A0543 A	0.1754 (13)	
050	05 32 23.42 −11 32 03.5	11.1	456.4	0.30 0.03	0.40 +0.05 −0.05	3.0e−02	0.63 0.07	6.35 0.73	A0545 A	0.1540 (4)	
051	05 33 14.02 −36 19 10.5	2.93	505.8	0.15 0.02	0.27 +0.07 −0.06	3.9e−03	0.35 0.08	0.33 0.08	S0535 A	0.0473 (13)	
052	05 38 15.36 −20 37 34.5	4.00	497.5	0.20 0.02	0.36 +0.08 −0.06	1.1e−03	0.47 0.09	1.69 0.33	A3358 A	0.0915 (14)	12
053	05 40 06.82 −40 50 30.5	3.53	601.0	0.43 0.03	0.70 +0.08 −0.07	1.0e−04	0.92 0.10	0.50 0.05	S0540 A	0.0358 (2)	
054	05 47 37.44 −31 52 30.0	1.95	579.3	0.31 0.02	0.47 +0.06 −0.05	1.2e−03	0.59 0.07	5.50 0.66	A3364 A	0.1483 (6)	
055	05 48 36.70 −25 28 27.0	1.88	553.8	0.26 0.02	0.75 +0.26 −0.18	3.9e−06	0.94 0.28	0.70 0.21	A0548 A	0.0416 (1)	
056	05 52 52.08 −21 03 20.5	4.33	529.0	0.33 0.03	0.53 +0.07 −0.06	5.3e−04	0.70 0.09	2.94 0.37	A0550 A	0.0990 (6)	
057	05 57 11.89 −37 28 26.0	3.95	705.1	0.21 0.02	0.38 +0.06 −0.05	2.3e−04	0.50 0.08	0.41 0.06	S0555 A	0.0440 (6)	
058	06 00 27.27 −48 46 02.0	5.68	993.4	0.27 0.02	0.29 +0.02 −0.02	4.1e−01	0.41 0.03		... C	...	13
059	06 01 37.77 −40 00 31.0	5.01	749.3	0.26 0.02	1.10 +0.38 −0.31	1.0e−08	1.50 2.69	2.15 2.38	A3376 A	0.0455 (2)	14
060	06 05 52.68 −35 18 08.0	4.30	714.7	0.38 0.02	0.46 +0.04 −0.04	8.7e−02	0.61 0.05	5.15 0.40	A3378 A	0.1410 (15)	15
061	06 21 44.17 −52 42 12.0	5.17	1038.3	0.14 0.01	0.30 +0.07 −0.06	5.3e−05	0.41 0.09	0.40 0.09	MS0620.6-5239 A	0.0480 (10)	
062	06 22 16.78 −64 56 31.5	5.57	3776.8	0.12 0.01	0.32 +0.05 −0.04	3.7e−11	0.44 0.06	0.11 0.02	S0585 A	0.0241 (2)	16

TABLE 1—*Continued*

Sequence	RA(J2000) Dec(J2000)	NH	Time	cr(5′) Err	cr(SRT) Err ±	P	F <sub>X</sub> Err	L <sub>X</sub> Err	ID Class	z Ref	Note
(1)	(2)	(3)	(4)	(5)	(6)	(7)	(8)	(9)	(10)	(11)	(12)
063	06 25 42.45 −37 15 02.0	7.08	720.8	0.08 0.01	0.27 +0.29 −0.11	2.6e−03	0.39 0.31	0.19 0.15	A3390 A	0.0338 (16)	17
064	06 26 20.10 −53 41 44.5	5.42	1185.9	0.39 0.02	0.95 +0.13 −0.11	1.5e−11	1.31 0.17	1.58 0.20	A3391 A	0.0531 (2)	
065	06 27 38.83 −54 26 38.5	5.42	1327.9	0.25 0.01	0.81 +0.21 −0.15	8.3e−11	1.12 0.25	1.19 0.27	A3395 A	0.0498 (2)	18
066	06 28 50.19 −41 43 32.5	6.27	633.1	0.23 0.02	0.26 +0.03 −0.03	3.2e−01	0.37 0.04	4.81 0.51	A3396 A	0.1759 (6)	
067	06 38 46.66 −53 58 22.0	6.57	861.7	0.28 0.02	0.36 +0.03 −0.03	2.7e−02	0.52 0.05	10.67 0.92	S0592 A	0.2216 (6)	
068	06 45 29.21 −54 13 17.5	6.57	723.8	0.24 0.02	0.35 +0.04 −0.04	2.8e−03	0.49 0.06	5.82 0.69	A3404 A	0.1670 (6)	
069	06 58 30.41 −55 56 47.0	6.34	507.8	0.35 0.03	0.51 +0.06 −0.06	2.2e−03	0.71 0.09	27.57 3.18	1ES 0657-558 A	0.2994 (6)	19
070	19 12 42.19 −75 17 24.0	6.68	218.9	0.26 0.04	0.33 +0.06 −0.06	1.2e−01	0.47 0.09	1.09 0.20	S0810 A	0.0736 (6)	
071	19 25 26.27 −42 57 12.5	6.59	301.0	0.25 0.03	0.40 +0.09 −0.08	1.0e−02	0.56 0.12	1.43 0.30	A3638 A	0.0774 (6)	
072	19 52 09.89 −55 03 18.5	4.86	191.1	0.20 0.04	0.43 +0.22 −0.14	1.3e−02	0.59 0.25	0.90 0.38	A3651 A	0.0599 (1)	
073	20 12 35.08 −56 50 30.5	4.59	174.9	0.91 0.07	2.44 +0.69 −0.50	1.6e−06	3.29 0.81	4.35 1.07	A3667 A	0.0556 (1)	
074	20 14 49.98 −24 30 35.0	7.40	367.1	0.20 0.03	0.28 +0.05 −0.05	3.1e−02	0.41 0.07	4.08 0.71	... B	0.1538 (6)	20
075	20 18 41.52 −52 42 28.5	4.72	346.3	0.29 0.03	0.55 +0.12 −0.10	7.1e−04	0.74 0.15	0.80 0.16	S0861 A	0.0504 (6)	
076	20 22 59.09 −20 57 25.0	5.59	179.6	0.16 0.04	0.25 +0.10 −0.08	7.1e−02	0.35 0.12	0.48 0.17	S0868 A	0.0564 (6)	21
077	20 34 19.52 −34 29 12.5	3.90	294.6	0.14 0.03	0.26 +0.11 −0.08	2.4e−02	0.35 0.13	1.24 0.45	A3693 A	0.0910 (1)	
078	20 34 41.41 −34 04 16.0	3.90	256.6	0.33 0.04	0.48 +0.09 −0.08	1.9e−02	0.64 0.11	2.35 0.41	A3694 A	0.0929 (17)	
079	20 34 46.86 −35 49 07.5	3.56	309.9	0.42 0.04	0.95 +0.24 −0.19	4.4e−05	1.25 0.28	4.24 0.96	A3695 A	0.0893 (1)	
080	21 02 10.33 −24 31 59.5	5.33	428.1	0.22 0.02	0.28 +0.04 −0.04	7.0e−02	0.38 0.06	5.70 0.81	EXO2059-247 A	0.1880 (18)	
081	21 04 19.81 −41 21 07.0	3.58	354.8	0.21 0.03	0.31 +0.06 −0.06	1.7e−02	0.40 0.08	4.72 0.89	A3739 A	0.1661 (6)	
082	21 04 51.57 −51 49 21.0	3.08	278.4	0.37 0.04	0.66 +0.14 −0.12	1.1e−03	0.85 0.16	0.88 0.17	ESO235-G050 B	0.0491 (19)	22
083	21 07 07.88 −25 26 40.5	5.52	427.9	0.13 0.02	0.30 +0.13 −0.09	3.5e−03	0.41 0.15	0.26 0.10	A3744 A	0.0381 (1)	

TABLE 1—*Continued*

Sequence	RA(J2000) Dec(J2000)	NH	Time	cr(5′) Err	cr(SRT) Err ±	P	F <sub>X</sub> Err	L <sub>X</sub> Err	ID Class	z Ref	Note
(1)	(2)	(3)	(4)	(5)	(6)	(7)	(8)	(9)	(10)	(11)	(12)
084	21 27 05.82 −12 10 12.5	4.78	390.8	0.17 0.02	0.28 +0.05 −0.05	2.9e−03	0.38 0.13	6.11 1.71	A2345 A	0.1760 (20)	
085	21 29 40.08 −00 05 49.5	4.22	286.0	0.28 0.03	0.35 +0.05 −0.05	8.8e−02	0.47 0.07		...	...	23
086	21 36 12.40 −62 22 24.5	3.21	388.4	0.55 0.04	0.67 +0.06 −0.06	7.1e−02	0.87 0.08		...	...	24
087	21 43 59.42 −56 37 31.0	3.42	353.1	0.35 0.03	0.50 +0.07 −0.07	9.3e−03	0.66 0.09	1.86 0.25	MRC2140-568 A	0.0815 (6)	
088	21 45 54.95 −10 06 24.5	4.03	258.8	0.20 0.03	0.38 +0.12 −0.09	8.4e−03	0.50 0.14	1.40 0.40	A2377 A	0.0808 (4)	
089	21 46 23.88 −57 17 22.5	2.57	355.8	0.24 0.03	0.42 +0.10 −0.08	2.4e−03	0.54 0.11	1.35 0.28	A3806 A	0.0765 (1)	
090	21 46 55.7 −43 53 21	1.77	312.7	0.27 0.03	0.49 +0.12 −0.10	1.6e−03	0.62 0.14	1.01 0.22	A3809 A	0.0620 (1)	
091	21 47 49.08 −46 00 02.0	2.72	304.7	0.20 0.03	0.30 +0.07 −0.06	2.1e−02	0.39 0.08	0.59 0.12	S0974 A	0.0596 (2)	
092	21 49 07.24 −30 41 52.5	2.31	370.1	0.26 0.03	0.32 +0.04 −0.04	9.4e−02	0.41 0.06	2.41 0.33	A3814 A	0.1177 (5)	
093	21 51 55.91 −15 43 19.0	4.27	250.8	0.11 0.02	0.31 +0.32 −0.14	1.7e−02	0.41 0.33	0.74 0.60	A2382 A	0.0648 (4)	
094	21 52 20.92 −19 33 54.5	3.05	349.8	0.36 0.03	0.73 +0.16 −0.13	1.1e−04	0.94 0.18	3.58 0.70	A2384 A	0.0943 (4)	
095	21 54 10.21 −57 52 05.5	2.12	362.7	0.44 0.04	0.87 +0.16 −0.13	3.0e−05	1.10 0.19	2.70 0.46	A3822 A	0.0759 (1)	
096	21 58 23.58 −60 25 40.0	2.77	375.2	0.19 0.02	0.50 +0.14 −0.12	5.3e−04	0.65 0.42	1.90 1.02	A3825 A	0.0751 (1)	
097	21 58 30.03 −09 47 54.5	4.00	327.4	0.21 0.03	0.35 +0.08 −0.07	7.6e−03	0.46 0.10	1.28 0.28	A2402 A	0.0806 (21)	
098	22 01 50.26 −22 25 53.5	2.61	250.9	0.13 0.03	0.29 +0.18 −0.10	1.7e−02	0.37 0.18	0.77 0.38	S0987 A	0.0701 (5)	
099	22 01 58.85 −59 57 37.0	2.84	372.0	0.69 0.04	1.18 +0.13 −0.12	2.9e−05	1.52 0.17	6.25 0.69	A3827 A	0.0984 (1)	
100	22 05 39.71 −05 35 00.5	4.68	323.7	0.30 0.03	0.44 +0.07 −0.07	1.1e−02	0.60 0.09	0.91 0.14	A2415 A	0.0597 (4)	
101	22 09 25.52 −51 50 37.5	2.06	348.8	0.17 0.02	0.31 +0.09 −0.07	6.4e−03	0.39 0.11	1.90 0.51	A3836 A	0.1065 (6)	
102	22 10 20.09 −12 10 49.0	3.87	286.7	0.45 0.04	0.89 +0.18 −0.15	1.1e−04	1.17 0.22	3.51 0.66	A2420 A	0.0838 (4)	
103	22 14 32.15 −10 22 23.0	3.86	288.7	0.47 0.04	0.68 +0.09 −0.09	5.4e−03	0.90 0.12	3.66 0.47	A2426 A	0.0978 (1)	
104	22 16 16.15	4.50	288.4	0.33	0.40	1.2e−01	0.54	1.65	A2428	0.0846	

TABLE 1—*Continued*

Sequence	RA(J2000) Dec(J2000)	NH	Time	cr(5′) Err	cr(SRT) Err ±	P	F <sub>X</sub> Err	L <sub>X</sub> Err	ID Class	z Ref	Note
(1)	(2)	(3)	(4)	(5)	(6)	(7)	(8)	(9)	(10)	(11)	(12)
	−09 20 11.0			0.04	+0.05 −0.05		0.07	0.22	A	(22)	
105	22 16 56.23 −17 25 25.5	2.28	283.0	0.24 0.03	0.31 +0.06 −0.05	6.6e−02	0.40 0.07	2.85 0.49	... A	0.1301 (8)	
106	22 17 45.58 −35 43 21.0	1.10	333.6	0.25 0.03	0.34 +0.05 −0.05	3.9e−02	0.42 0.06	3.84 0.59	A3854 A	0.1474 (5)	
107	22 18 07.76 −65 12 00.0	2.83	446.7	0.28 0.03	0.43 +0.07 −0.06	3.2e−03	0.55 0.08	2.11 0.31	... A	0.0951 (6)	25
108	22 18 12.49 −03 47 59.0	5.73	253.6	0.18 0.03	0.38 +0.17 −0.11	8.2e−03	0.52 0.20	1.80 0.69	MS2215.7-0404 A	0.0900 (10)	26
109	22 18 40.71 −38 53 46.5	1.33	330.9	0.28 0.03	0.44 +0.08 −0.07	4.7e−03	0.54 0.09	3.67 0.63	A3856 A	0.1260 (23)	
110	22 20 33.87 −35 09 52.0	1.09	327.6	0.43 0.04	0.55 +0.06 −0.06	4.9e−02	0.67 0.07	6.77 0.75	A3866 B	0.1544 (6)	27
111	22 23 48.91 −01 39 25.0	5.34	237.9	0.29 0.04	0.63 +0.21 −0.15	1.4e−03	0.87 0.25	3.03 0.89	A2440 A	0.0904 (4)	
112	22 24 31.31 −55 15 15.0	3.54	362.3	0.15 0.02	0.28 +0.09 −0.07	8.8e−03	0.36 0.10	0.95 0.27	APM222041.3-552 A	0.0780 (24)	
113	22 27 52.46 −30 34 10.5	1.09	312.6	0.42 0.04	0.53 +0.06 −0.06	5.7e−02	0.65 0.08	0.90 0.10	A3880 A	0.0570 (23)	
114	22 28 55.32 −60 54 24.5	2.22	458.9	0.13 0.02	0.27 +0.10 −0.07	4.6e−03	0.34 0.11	0.24 0.08	ESO146-G028 A	0.0412 (25)	
115	22 34 28.50 −37 43 53.5	1.20	258.2	0.48 0.04	0.69 +0.09 −0.09	8.0e−03	0.85 0.11	8.20 1.08	A3888 A	0.1510 (26)	
116	22 35 39.73 −01 29 02.5	5.81	166.6	0.24 0.04	0.36 +0.10 −0.09	4.0e−02	0.51 0.13	0.77 0.20	A2457 A	0.0597 (4)	
117	22 46 17.79 −52 43 48.0	1.52	411.1	0.31 0.03	0.48 +0.07 −0.07	2.1e−03	0.60 0.09	2.43 0.35	A3911 A	0.0974 (27)	
118	22 48 44.45 −44 31 50.0	1.79	250.2	0.38 0.04	0.52 +0.08 −0.07	2.8e−02	0.65 0.09	17.18 2.49	S1063 B	0.2520 <sup>a</sup> (2)	
119	22 50 03.61 −64 26 30.0	2.80	469.6	0.42 0.03	0.93 +0.20 −0.18	1.1e−06	1.20 0.23	4.69 0.87	A3921 A	0.0936 (1)	
120	22 54 01.45 −63 15 02.0	2.23	400.2	0.19 0.02	0.28 +0.06 −0.05	1.6e−02	0.35 0.07	6.62 1.24	AM2250-633 A	0.2112 (6)	
121	22 54 27.79 −58 06 41.5	2.12	404.7	0.11 0.02	0.27 +0.17 −0.09	7.3e−03	0.35 0.17		... C	...	28
122	23 13 58.42 −42 43 47.0	1.85	202.4	0.87 0.07	1.07 +0.10 −0.10	7.0e−02	1.34 0.13	1.93 0.18	S1101 A	0.0580 (10)	
123	23 15 42.49 −02 22 27.0	4.18	343.1	0.19 0.03	0.30 +0.07 −0.06	1.2e−02	0.40 0.08	0.12 0.03	ZWIII99 A	0.0267 (8)	29
124	23 21 36.11 −41 53 37.0	1.96	164.7	0.29 0.04	0.52 +0.16 −0.13	1.1e−02	0.66 0.18	2.23 0.62	A3998 A	0.0890 (10)	



TABLE 1—*Continued*

Sequence	RA(J2000) Dec(J2000)	NH	Time	cr(5′) Err	cr(SRT) Err ±	P	F <sub>X</sub> Err	L <sub>X</sub> Err	ID Class	z Ref	Note
(1)	(2)	(3)	(4)	(5)	(6)	(7)	(8)	(9)	(10)	(11)	(12)
125	23 25 18.95 −12 07 32.0	2.50	332.3	0.87 0.05	1.06 +0.08 −0.08	5.6e−02	1.36 0.10	4.21 0.31	A2597 A	0.0852 (4)	30
126	23 44 15.98 −04 22 24.5	3.54	339.8	0.40 0.04	0.93 +0.23 −0.18	1.8e−05	1.21 0.27	3.20 0.71	... A	0.0786 (8)	
127	23 47 41.78 −28 08 26.5	1.55	334.1	1.30 0.06	2.21 +0.19 −0.18	2.0e−06	2.75 0.23	1.01 0.08	A4038 A	0.0292 (1)	
128	23 51 40.36 −26 04 54.0	1.66	329.8	0.43 0.04	0.52 +0.06 −0.06	8.8e−02	0.66 0.07	14.10 1.51	A2667 A	0.2264 (8)	31
129	23 54 12.70 −10 24 57.0	2.92	317.9	0.34 0.03	0.60 +0.11 −0.10	7.8e−04	0.78 0.14	1.92 0.34	A2670 A	0.0762 (1)	
130	23 57 00.02 −34 45 24.5	1.10	350.6	0.96 0.05	1.61 +0.15 −0.15	1.3e−05	1.97 0.18	1.79 0.17	A4059 A	0.0460 (10)	

<sup>a</sup>This is an estimated redshift.

NOTE.—Notes on single sources: **1.** – cluster in Strubble & Rood (1991); **2.** – identified as galaxy MS0122.9+0129 in Maccacaro et al. (1994), extended from ROSAT HRI and PSPC pointed observations, many small galaxies nearby,  $z$  measured from 3 galaxies; **3.** – central galaxy is radio source (Brinkman, Siebert & Boller 1994),  $z$  measured from 3 galaxies; **4.** – X-ray emission slightly elongated towards cluster A3016; **5.** – source at low  $z$  (measured on 2 galaxies) but pointlike, several other objects in vicinity, could be a group or a single galaxy, uncertain identification; **6.** – extended in HRI observation,  $z$  measured from 2 galaxies, RASS data slightly elongated towards a pointlike source at 02h32m37.5s -44d21m51s (J2000); **7.** – double peaked X-ray emission, SRT count rate underestimated because the RASS ML position is centered on one peak,  $0.61 \pm 0.01$  cts/s hard count rate from PSPC pointed observations; **8.** – extended in HRI observation, identified as normal galaxy in Einstein Catalog IPC Slew Survey but is cluster (4 galaxies with consistent  $z$ ); **9.** – extended in HRI observation, paired with IC366 at  $3.2'$ , flagged as nearby galaxy group in Lyon-Meudon catalog (Garcia 1993) on the basis of a percolation method,  $z$  available only for central galaxy NGC1550; **10.** – normal galaxy NGC1650 in rich field, likely galaxy group, only one  $z$  available; **11.** –  $z$  measured from 4 galaxies; **12.** – cluster behind star HD37493 (spectral type K0,  $m_V = 8.2$ ), which could only slightly contribute to the X-ray emission (see Maccacaro et al. 1988), the extended X-ray emission implies that most of the emission comes from the cluster; **13.** – unconfirmed cluster with no spectroscopic information available; **14.** – elongated X-ray emission between 2 bright galaxies, SRT count rate in agreement with hard count rate from PSPC pointed observation; **15.** – extended in HRI observation; **16.** – also A3389 (optical position at  $3.3'$  from X-ray peak), double peaked X-ray emission centered on NGC 2235 (at  $0.7'$ ); **17.** – double peaked X-ray emission, RASS ML position centered on one peak,  $0.27 \pm 0.01$  cts/s hard count rate from PSPC pointed observation; **18.** – double peaked X-ray emission, RASS ML position centered on one peak,  $1.16 \pm 0.03$  cts/s hard count rate from PSPC pointed observation; **19.** – extended in HRI observation, classified as galaxy cluster in Tucker, Tananbaum & Remillard (1995); **20.** – probable cluster with only one  $z$  measured; **21.** – central galaxy is radio source (Brinkman, Siebert & Boller 1994, Douglas et al. 1996),  $z$  measured from 2 galaxies; **22.** – extended in HRI observation, probable group,  $z$  only from the brightest galaxy; **23.** – extended in HRI observation, no spectroscopic information available; **24.** – unidentified candidate with no spectroscopic information available; **25.** –  $z$  measured from 5 galaxies; **26.** – MS2215.70404 (coincident with RASS ML emission peak) and MS2216.00401 are two separate sources probably parts of the extended X-ray emission from a single cluster (Gioia & Luppino 1994); **27.** – extended in HRI observation, only one  $z$  measured; **28.** – probable cluster, no spectroscopic information available; **29.** – extended in HRI observation, paired with NGC7556,  $z$  measured from 2 galaxies; **30.** – extended in HRI observation; **31.** – extended in HRI observation.

REFERENCES.— (1) Mazure et al. 1996; (2) Abell et al. 1989; (3) Dalton et al. (1997); (4) Strubble & Rood 1987; (5) Collins et al. 1995; (6) data from the ESOKP collaboration; (7) Zabludoff et al. 1993; (8) data from the South Galactic Pole survey (see Romer et al. 1994); (9) Crawford et al. 1995; (10) Stocke et al. 1991; (11) de Vaucouleurs et al. 1991; (12) Huchra et al. 1993; (13) Quintana & Ramirez 1995; (14) Henry & Mullir 1997, priv. comm.; (15) Ebeling et al. 1996; (16) Galli et al. 1993; (17) Muriel, Nicotra & Lambas 1990; (18) NED11 1992; (19) Lauberts & Valentijn 1989; (20) Ledlow & Owen 1995; (21) Postman, Huchra & Geller 1992; (22) Allen et al. 1992; (23) Ebeling & Maddox 1995; (24) Dalton et al. 1994; (25) Muriel, Nicotra & Lambas 1995; (26) Teague et al. 1990; (27) Postman & Lauer 1995.

TABLE 2  
REJECTED CLUSTER CANDIDATES

Source ID	RA (J2000)	Dec (J2000)	$F_X$ $10^{-11}$ cgs	$F_X$ Err $10^{-11}$ cgs	Type
HD3237	00 35 08.17	-50 20 05.5	0.61	0.08	STA
NGC0253	00 47 32.70	-25 17 21.0	0.45	0.07	GAL
G60	01 35 00.88	-29 54 40.0	1.54	0.06	STA
	02 27 16.47	+02 01 55.5	1.10	0.08	AGN
2A0311-227	03 14 12.88	-22 35 41.5	1.81	0.11	STA
MRK0609	03 25 26.58	-06 08 20.5	0.45	0.04	AGN
HR1325	04 15 22.25	-07 38 56.5	0.51	0.07	STA
H0449-55	04 53 31.51	-55 52 01.0	0.79	0.05	STA
HR702	05 12 55.25	-16 12 19.5	0.35	0.06	STA
NGC1851	05 14 06.18	-40 02 31.0	2.87	0.10	GC
0548-322	05 50 40.53	-32 16 17.5	2.04	0.08	AGN
HD45081	06 18 27.59	-72 02 40.5	0.74	0.04	STA
HR2326	06 23 57.31	-52 41 43.0	0.50	0.04	STA
PMNJ1931-2635	19 31 50.01	-26 34 31.5	0.45	0.09	AGN
PKS1930-510	19 34 51.95	-50 52 54.0	0.50	0.54	GAL
HR7571	19 53 06.63	-14 36 08.0	0.44	0.06	STA
PKS2005-489	20 09 25.07	-48 49 48.0	1.62	0.09	AGN
PKS2035-714	20 40 06.08	-71 14 53.0	0.35	0.06	AGN
	20 41 49.71	-37 33 45.0	0.57	0.10	GAL <sup>a</sup>
HD205249	21 34 16.18	-13 29 07.5	0.54	0.07	STA
PMNJ2150-1411	21 50 15.62	-14 10 45.0	0.85	0.10	AGN
ESO075-G041	21 56 54.04	-69 40 34.5	0.38	0.06	AGN
SAO145804	22 00 36.51	-02 44 27.0	5.86	0.22	STA
[HB89]2227-399	22 30 39.28	-39 42 54.0	0.39	0.05	AGN
NGC7603	23 18 56.18	+00 14 38.5	0.40	0.04	AGN
HD220054	23 21 52.89	-69 42 18.0	0.40	0.07	STA
HD220186	23 21 55.46	-10 50 03.0	0.56	0.06	STA

NOTE.—Units of right ascension are hours, minutes, and seconds, and units of declination are degrees, arcminutes, and, arcseconds. See text for explanation of types.

<sup>a</sup>Identification based on ROSAT HRI and COSMOS data.

TABLE 3  
 “MISSED” ACO CLUSTERS

Name	RA(J2000) [deg]	Dec(J2000) [deg]	$cr_{SASS1}$ [1-2.4 keV]	z	Ref.
A0194	21.3867	-1.5069	0.045	0.0178	(1)
A0514	71.9158	-20.4290	0.026	0.0730	(1)
A3164	56.4567	-57.0456	...	0.0611	(2)
A3223	62.1429	-30.8189	0.036	0.0601	(3)
A3716	312.8858	-52.7122	0.051	0.0456	(2)
A3733	315.4387	-28.0283	0.034	0.0386	(2)

REFERENCES.— (1) Struble & Rood 1987; (2) Abell et al. 1989; (3) den Hartog & Katgert 1996.